

## Electronic Supplementary Information for

# Novel Anti-Kasha Fluorophores Exhibiting Dual Emission with Thermally Activated Delayed Fluorescence Through Detouring Triplet Manifolds

Byung Hak Jhun,<sup>a,b</sup> Dong Yeun Jeong,<sup>a</sup> Sanghee Nah,<sup>c</sup> Soo Young Park,<sup>\*b</sup> and Youngmin You<sup>\*a</sup>

<sup>a</sup>Division of Chemical Engineering and Materials Science, and Graduate Program in System Health Science and Engineering,, Ewha Womans University, Seoul 03760, Republic of Korea.

e-mail: [odds2@ewha.ac.kr](mailto:odds2@ewha.ac.kr)

<sup>b</sup>Center for Supramolecular Optoelectronic Materials (CSOM) and Department of Materials Science and Engineering, Seoul National University, Seoul 08826, Republic of Korea.

e-mail: [parksy@snu.ac.kr](mailto:parksy@snu.ac.kr)

<sup>c</sup>Seoul Center, Korea Basic Science Institute (KBSI), Seoul 02841, Republic of Korea..

## CONTENTS

---

<b>Experimental Details</b>	S6
<b>Table S1.</b> Photophysical parameters of thermally activated delayed fluorescence emissions	S13
<b>Table S2.</b> One-electron oxidation and reduction potentials and the driving force for photoinduced intramolecular electron transfer	S14
<b>Table S3.</b> Energy levels of the charge-separated species ( $E(\text{CS})$ ), the emissive singlet ICT states ( $E(^1\text{ICT})$ ), and the triplet $n-\pi^*$ transition state ( $E(^3n-\pi^*)$ ).	S15
<b>Table S4.</b> TD-DFT calculation results for the pseudo-equatorial conformers of the dyads obtained with the different functionals	S16
<b>Table S5.</b> TD-DFT calculation results for the pseudo-axial conformers of the	S17

	dyads obtained with the different functionals	
<b>Table S6.</b>	Report of the Cartesian coordinates of the optimized geometry of CzC	S18
<b>Table S7.</b>	Report of the Cartesian coordinates of the optimized geometry of the pseudo-axial conformer of AZPC	S19
<b>Table S8.</b>	Report of the Cartesian coordinates of the optimized geometry of the pseudo-equatorial conformer of AZPC	S20
<b>Table S9.</b>	Report of the Cartesian coordinates of the optimized geometry of the pseudo-axial conformer of spiroACC	S21
<b>Table S10.</b>	Report of the Cartesian coordinates of the optimized geometry of the pseudo-equatorial conformer of spiroACC	S23
<b>Table S11.</b>	Report of the Cartesian coordinates of the optimized geometry of the pseudo-axial conformer of DMACC	S25
<b>Table S12.</b>	Report of the Cartesian coordinates of the optimized geometry of the pseudo-equatorial conformer of DMACC	S26
<b>Table S13.</b>	Report of the Cartesian coordinates of the optimized geometry of the pseudo-axial conformer of PXZC	S27
<b>Table S14.</b>	Report of the Cartesian coordinates of the optimized geometry of the pseudo-equatorial conformer of PXZC	S28
<b>Table S15.</b>	Report of the Cartesian coordinates of the optimized geometry of the pseudo-axial conformer of PTZC	S29
<b>Table S16.</b>	Report of the Cartesian coordinates of the optimized geometry of the pseudo-equatorial conformer of PTZC	S30
<b>Table S17.</b>	Summary of the TD-B3LYP calculation results for CzC	S31
<b>Table S18.</b>	Summary of the TD-B3LYP calculation results for the pseudo-axial conformer of AZPC	S32
<b>Table S19.</b>	Summary of the TD-B3LYP calculation results for the pseudo-equatorial conformer of AZPC	S33
<b>Table S20.</b>	Summary of the TD-B3LYP calculation results for the pseudo-axial conformer of spiroACC	S34
<b>Table S21.</b>	Summary of the TD-B3LYP calculation results for the pseudo-equatorial conformer of spiroACC	S35
<b>Table S22.</b>	Summary of the TD-B3LYP calculation results for the pseudo-axial conformer of DMACC	S36
<b>Table S23.</b>	Summary of the TD-B3LYP calculation results for the pseudo-equatorial conformer of DMACC	S37
<b>Table S24.</b>	Summary of the TD-B3LYP calculation results for the pseudo-axial conformer of PXZC	S38
<b>Table S25.</b>	Summary of the TD-B3LYP calculation results for the pseudo-equatorial conformer of PXZC	S39
<b>Table S26.</b>	Summary of the TD-B3LYP calculation results for the pseudo-axial	S40

	conformer of PTZC	
<b>Table S27.</b>	Summary of the TD-B3LYP calculation results for the pseudo-equatorial conformer of PTZC	S41
<b>Table S28.</b>	Crystallographic data and selected bond distances (Å) and angles (°) of PTZC	S42
<b>Fig. S1</b>	Correlation between optical ( $E_g^{\text{opt}}$ ) and electrochemical ( $E_g^{\text{elec}}$ ) band gap energies (i.e., $e \cdot [E_{\text{red}} - E_{\text{ox}}]$ ) of the dyads	S45
<b>Fig. S2</b>	The Lippert-Mataga plots of the fluorescence emission of PC, CzC, AZPC, spiroACC, DMACC, PXZC, and PTZC: Empty squares, short-wavelength emission; filled squares, long-wavelength emission. Solvent polarity parameter ( $f$ ): 0.0135 (toluene), 0.148 (chloroform), 0.200 (ethyl acetate), 0.210 (2-methyltetrahydrofuran), 0.218 (dichloromethane), 0.275 ( <i>N,N'</i> -dimethylformamide), and 0.305 (acetonitrile).	S46
<b>Fig. S3</b>	Photoluminescence decay traces of the short- (blue) and long-wavelength (red) emissions of dyads (50 μM in Ar-saturated toluene) obtained after pulsed laser excitation at 345 nm. (a) CzC, (b) AZPC, (c) spiroACC, (d) DMACC, (e) PXZC, and (f) PTZC. The black curves show non-linear least-squares fits of the decay traces to a multi-exponential decay model. Fit results are summarized in Table 1 in the main text	S47
<b>Fig. S4</b>	(a) Photoluminescence decay traces of the long-wavelength emissions of dyads (50 μM in Ar-saturated toluene) obtained after picosecond pulsed laser excitation at 377 nm. (b) Time-resolved emission spectrum of PTZC (50 μM in Ar-saturated toluene) obtained after picosecond pulsed laser excitation at 377 nm	S48
<b>Fig. S5</b>	Photoluminescence spectra of the dyads (10 μM in toluene) obtained before (black) and after (red) deaeration: (a) CzC, (b) AZPC, (c) spiroACC, (d) DMACC, (e) PXZC, and (f) PTZC. The gray and orange dotted lines in (c) indicate convoluted spectra of the long- and short-wavelength emissions, respectively	S49
<b>Fig. S6</b>	Photolumiensiunce decay traces of the LW emission of dyads (50 μM in Ar-saturated toluene) obtained before (black) and after (red) deaeration under pulsed laser excitation at 377 nm. (a) CzC, (b) AZPC, (c) spiroACC, (d) DMACC, (e) PXZC, and (f) PTZC	S50
<b>Fig. S7</b>	Variable-temperature fluorescence decay traces of the LW emission of (a) PXZC and (b) PTZC (5 wt % in poly(methyl methacrylate) films) acquired after 377 nm pulsed laser excitation (temporal resolution, 16 ns)	S51
<b>Fig. S8</b>	Phosphorescence spectra of dyads (50 μM in iodoethane or 2-MeTHF) recorded after 10 ms delay at 77 K	S52
<b>Fig. S9</b>	Femtosecond transient absorption spectra of toluene solutions containing (a) PC and (b) DMACC recorded after femtosecond pulsed laser excitation at 350 nm.	S53
<b>Fig. S10</b>	UV–Vis–NIR absorption difference spectra of 2.0 mM DMACC (Ar-	S54

saturated acetonitrile containing 0.10 M TBAPF<sub>6</sub> supporting electrolyte) recorded upon application of an anodic potential of 0.50–0.78 V vs Ag<sup>+</sup>/Ag (scan rate = 0.4 mV s<sup>-1</sup>). A Pt mesh and a Pt wire were used for the working and counter electrodes, respectively. An Ag/AgNO<sub>3</sub> pseudo reference electrode was used.

<b>Fig. S11</b>	Optimized (B3LYP/6-311+G(d,p)) geometries and their energies of pseudo-axial (ax) and pseudo-equatorial (eq) conformations of (a) CzC, (b) AZPC, (c) spiroACC, (d) DMACC, (e) PXZC, and (f) PTZC. The energy value is indicated relatively to that of the lower-energy conformer	S55
<b>Fig. S12</b>	Isosurface plots (isovalue = 0.02) of several molecular orbitals of CzC	S56
<b>Fig. S13</b>	Isosurface plots (isovalue = 0.02) of several molecular orbitals of the pseudo-axial conformer of AZPC	S57
<b>Fig. S14</b>	Isosurface plots (isovalue = 0.02) of several molecular orbitals of the pseudo-equatorial conformer of AZPC	S58
<b>Fig. S15</b>	Isosurface plots (isovalue = 0.02) of several molecular orbitals of the pseudo-axial conformer of spiroACC	S59
<b>Fig. S16</b>	Isosurface plots (isovalue = 0.02) of several molecular orbitals of the pseudo-equatorial conformer of spiroACC	S60
<b>Fig. S17</b>	Isosurface plots (isovalue = 0.02) of several molecular orbitals of the pseudo-axial conformer of DMACC	S61
<b>Fig. S18</b>	Isosurface plots (isovalue = 0.02) of several molecular orbitals of the pseudo-equatorial conformer of DMACC	S62
<b>Fig. S19</b>	Isosurface plots (isovalue = 0.02) of several molecular orbitals of the pseudo-axial conformer of PXZC	S63
<b>Fig. S20</b>	Isosurface plots (isovalue = 0.02) of several molecular orbitals of the pseudo-equatorial conformer of PXZC	S64
<b>Fig. S21</b>	Isosurface plots (isovalue = 0.02) of several molecular orbitals of the pseudo-axial conformer of PTZC	S65
<b>Fig. S22</b>	Isosurface plots (isovalue = 0.02) of several molecular orbitals of the pseudo-equatorial conformer of PTZC	S66
<b>Fig. S23</b>	Comparison between optimized (B3LYP/6-311+G(d,p)) geometries of D–C dyads in ground state (magenta) and first singlet excited state (blue). Dihedral angle between cyclic amino donor and coumarin scaffold of both states also described in the Figure	S67
<b>Fig. S24</b>	Photoluminescence decay traces of LW emission for deoxygenated 50 μM toluene solution and determination of ratio between prompt fluorescence and delayed fluorescence using ratio of emission area: (a) spiroACC, (b) DMACC, (c) PXZC, and (d) PTZC.	S68
<b>Fig. S25</b>	<sup>1</sup> H NMR (300 MHz, CDCl <sub>3</sub> ) spectrum of CzC	S69
<b>Fig. S26</b>	<sup>13</sup> C{ <sup>1</sup> H} NMR (126 MHz, CDCl <sub>3</sub> ) spectrum of CzC	S70

<b>Fig. S27</b>	$^1\text{H}$ NMR (300 MHz, $\text{CDCl}_3$ ) spectrum of AZPC	S71
<b>Fig. S28</b>	$^{13}\text{C}\{\text{H}\}$ NMR (126 MHz, $\text{CDCl}_3$ ) spectrum of AZPC	S72
<b>Fig. S29</b>	$^1\text{H}$ NMR (300 MHz, $\text{CDCl}_3$ ) spectrum of spiroACC	S73
<b>Fig. S30</b>	$^{13}\text{C}\{\text{H}\}$ NMR (126 MHz, $\text{CDCl}_3$ ) spectrum of spiroACC	S74
<b>Fig. S31</b>	$^1\text{H}$ NMR (300 MHz, $\text{CDCl}_3$ ) spectrum of DMACC	S75
<b>Fig. S32</b>	$^{13}\text{C}\{\text{H}\}$ NMR (126 MHz, $\text{CDCl}_3$ ) spectrum of DMACC	S76
<b>Fig. S33</b>	$^1\text{H}$ NMR (300 MHz, $\text{CDCl}_3$ ) spectrum of PXZC	S77
<b>Fig. S34</b>	$^{13}\text{C}\{\text{H}\}$ NMR (126 MHz, $\text{CDCl}_3$ ) spectrum of PXZC	S78
<b>Fig. S35</b>	$^1\text{H}$ NMR (300 MHz, $\text{CDCl}_3$ ) spectrum of PTZC	S79
<b>Fig. S36</b>	$^{13}\text{C}\{\text{H}\}$ NMR (126 MHz, $\text{CDCl}_3$ ) spectrum of PTZC	S80
<b>References</b>		S81

---

## Experimental Details

**Materials and General Methods.** Commercially available chemicals were used as received without further purification. All glassware, syringes, and magnetic stir bars were dried in a convection oven. Reactions were monitored through thin layer chromatography (TLC) technique using a commercially available TLC plate (silica gel 254, Merck Co.). Purification through silica gel column chromatography was performed with silica gel 60G (particle size 5–40 µm, Merck Co.).  $^1\text{H}$  NMR and  $^{13}\text{C}\{^1\text{H}\}$  NMR spectra were collected using Bruker, Avance-300 and 500 NMR spectrometers and referenced to tetramethylsilane. High-resolution mass spectra were acquired using JEOL, JMS-700GC or Agilent, 6890 series instruments. Elemental analyses were performed using a Thermo Fisher Scientific, Flash 2000 instrument. Poly(methyl methacrylate) (PMMA) was purchased from Merck Co. ( $\text{Mw} \sim 15,000$ ) and used as received. 1,2-Dichloroethane containing 10 wt % of PMMA and dyads (5 wt % relative to PMMA) were spincoated onto 2 cm × 2 cm quartz plates after passed through a syringe filter (pore size = 0.50 µm), using an EPLEX, SPIN-1200D spin coater. Syntheses of 7-bromocoumarin,<sup>[1]</sup> PC,<sup>[1]</sup> 2-bromo-N-phenylaniline<sup>[2]</sup>, and SPAC<sup>[3]</sup> were described previously.

**Synthesis of CzC.** 7-Bromocoumarin (0.300 g, 1.33 mmol), carbazole (0.268 g, 1.60 mmol), (*1R*)-*trans*-1,2-cyclohexanediamine (0.030 g, 0.27 mmol), Cul (0.025 g, 0.13 mmol), and K<sub>3</sub>PO<sub>4</sub> (0.593 g, 2.79 mmol) were added to a 50 mL round-bottom flask. The reaction mixture was dissolved in 25 mL of anhydrous toluene, and refluxed for 14 h under an Ar atmosphere. The reaction mixture was cooled down to room temperature, and poured onto water, followed by extracted with CH<sub>2</sub>Cl<sub>2</sub> (150 mL × four times). The organic layer was collected, dried over MgSO<sub>4</sub>, and filtered. Silica gel column chromatography with CH<sub>2</sub>Cl<sub>2</sub>:*n*-hexane = 1:4 (v/v) gave ivory powders in a 82% yield.  $^1\text{H}$  NMR (300 MHz, CDCl<sub>3</sub>)  $\delta$ : 6.51 (d, *J* = 9.0 Hz, 1H), 7.34 (td, *J* = 9.0 Hz, 2H), 7.44 (td, *J* = 9.0 Hz, 2H), 7.51–7.53 (m, 3H), 7.62 (d, *J* = 3.0 Hz, 1H), 7.72 (d, *J* = 9.0 Hz, 1H), 7.81 (d, *J* = 12 Hz, 1H), 8.15 (d, *J* = 6.0 Hz, 2H).  $^{13}\text{C}\{^1\text{H}\}$  NMR (126 MHz, CDCl<sub>3</sub>)  $\delta$ : 109.88, 114.78, 116.73, 117.70, 120.73, 121.08, 122.75, 124.14, 126.54, 129.32, 140.24, 141.30, 143.02, 155.31, 160.50. HR MS (FAB<sup>+</sup>, *m*-NBA): calcd for C<sub>21</sub>H<sub>14</sub>NO<sub>2</sub> ([M+H]<sup>+</sup>), 312.1025; found, 312.1030. Anal. calcd for C<sub>21</sub>H<sub>13</sub>NO<sub>2</sub>: C, 81.01; H, 4.21; N, 4.50. Found: C, 80.11; H, 4.13; N, 4.42.

**Synthesis of AZPC.** To a flame-dried 50 mL one-necked round-bottom flask, 7-bromocoumarin (0.300 g, 1.33 mmol), 10,11-dihydro-5*H*-dibenzo[*b,f*]azepine (0.286 g, 1.46 mmol), and NaOtBu (0.256 g, 2.66 mmol) were added and dissolved in 20 mL of anhydrous toluene. Pd(PtBu<sub>3</sub>)<sub>2</sub> (0.068 g, 0.13 mmol) was subsequently added to the flask under an Ar atmosphere. The reaction mixture was refluxed for 24 h. The cooled reaction mixture was poured onto water, and extracted with CH<sub>2</sub>Cl<sub>2</sub> (100 mL × four times). The organic layer was dried over MgSO<sub>4</sub>, filtered, and concentrated under vacuum. Silica gel column chromatography was performed using ethylacetate:*n*-hexane = 1:4 (v/v) as an eluent to furnish white powders in a 33% yield. <sup>1</sup>H NMR (300 MHz, CDCl<sub>3</sub>) δ: 3.00 (s, 4H), 6.08 (d, *J* = 9.0 Hz, 1H), 6.47 (dd, *J* = 3.0 Hz, 1H), 6.51 (d, *J* = 3.0 Hz, 1H), 7.15 (d, *J* = 9.0 Hz, 1H), 7.27–7.29 (m, 6H), 7.35–7.39 (m, 2H), 7.53 (d, *J* = 9.0 Hz, 1H). <sup>13</sup>C{<sup>1</sup>H} NMR (126 MHz, CDCl<sub>3</sub>) δ: 30.80, 99.84, 110.04, 110.42, 110.92, 127.67, 128.19, 128.65, 129.39, 131.43, 137.97, 142.45, 143.69, 152.55, 156.24, 162.01. HR MS (FAB<sup>+</sup>, *m*-NBA): calcd for C<sub>23</sub>H<sub>18</sub>NO<sub>2</sub> ([M+H]<sup>+</sup>), 340.1338; found, 340.1339. Anal. calcd for C<sub>21</sub>H<sub>13</sub>NO<sub>2</sub>: C, 81.40; H, 5.05; N, 4.13. Found: C, 81.19; H, 3.83; N, 4.09.

**Synthesis of spiroACC.** SpiroACC was prepared following the procedure used for the synthesis of AZPC, except employing SPAC in place of 10,11-dihydro-5*H*-dibenzo[*b,f*]azepine. Silica gel column chromatography using chloroform:*n*-hexane = 2:1 (v/v) as an eluent gave yellow powders in a 32% yield. <sup>1</sup>H NMR (300 MHz, CDCl<sub>3</sub>) δ: 6.37 (d, *J* = 9.0 Hz, 2H), 6.44 (d, *J* = 9.0 Hz, 2H), 6.55–6.63 (m, 3H), 6.94 (t, *J* = 6.0 Hz, 2H), 7.29 (s, 2H), 7.37–7.46 (m, 5H), 7.54 (s, 1H), 7.80–7.88 (m, 4H). <sup>13</sup>C{<sup>1</sup>H} NMR (126 MHz, CDCl<sub>3</sub>) δ: 114.62, 117.68, 119.14, 119.88, 120.18, 120.23, 121.41, 124.53, 125.35, 125.90, 127.01, 127.27, 127.54, 127.69, 127.91, 128.23, 128.63, 130.55, 139.45, 140.81, 142.92, 144.76, 156.12, 156.47, 160.24. HR MS (FAB<sup>+</sup>, *m*-NBA): calcd for C<sub>34</sub>H<sub>22</sub>NO<sub>2</sub> ([M+H]<sup>+</sup>), 476.1651; found, 476.1653. Anal. calcd for C<sub>21</sub>H<sub>13</sub>NO<sub>2</sub>: C, 85.87; H, 4.45; N, 2.95. Found: C, 78.12; H, 4.27; N, 2.55.

**Synthesis of DMACC.** 7-Bromocoumarin (0.300 g, 1.33 mmol), 9,9-dimethyl-9,10-dihydroacridine (0.334 g, 1.60 mmol), K<sub>2</sub>CO<sub>3</sub> (0.885 g, 6.40 mmol) were added into a one-necked 100 mL round-bottom flask. Dry toluene was delivered to the flask under an Ar atmosphere. Pd(PtBu<sub>3</sub>)<sub>2</sub> (0.068 g, 0.13 mmol) was added quickly into the reaction

mixture which was refluxed for 24 h under an Ar atmosphere. After cooling to room temperature, the reaction mixture was poured onto water and extracted using  $\text{CH}_2\text{Cl}_2$ . The organic layer was dried over  $\text{MgSO}_4$ , filtered, and concentrated under vacuum. Silica gel column chromatography was performed using ethylacetate:*n*-hexane = 1:3 (v/v), and subsequent recrystallization in methanol:chloroform gave needle-shaped yellow crystals in a 53% yield.  $^1\text{H}$  NMR (300 MHz,  $\text{CD}_2\text{Cl}_2$ )  $\delta$ : 1.67 (s, 6H), 6.32–6.38 (m, 2H), 6.47 (d,  $J$  = 9.6 Hz, 1H), 6.93–7.02 (m, 4H), 7.27 (dd,  $J$  = 8.1 Hz, 1H), 7.35 (d,  $J$  = 1.8 Hz, 1H), 7.45–7.51 (m, 2H), 7.75 (d,  $J$  = 8.4 Hz, 1H), 7.83 (d,  $J$  = 9.3 Hz, 1H).  $^{13}\text{C}\{\text{H}\}$  NMR (126 MHz,  $\text{CDCl}_3$ )  $\delta$ : 31.13, 36.36, 114.93, 117.10, 118.42, 118.86, 121.72, 125.60, 126.56, 126.65, 130.22, 131.49, 140.49, 142.97, 145.24, 155.97, 160.42. HR MS (FAB $^+$ , *m*-NBA): calcd for  $\text{C}_{24}\text{H}_{20}\text{NO}_2$  ( $[\text{M}+\text{H}]^+$ ), 354.1494; found, 354.1492. Anal. calcd for  $\text{C}_{24}\text{H}_{19}\text{NO}_2$ : C, 81.56; H, 5.42; N, 3.96. Found: C, 81.50; H, 5.41; N, 3.99.

**Synthesis of PXZC.** PXZC was prepared following the procedures identical to the synthesis of DMACC, except using 10*H*-phenoxazine in place of 9,9-dimethyl-9,10-dihydroacridine. Silica gel column chromatography using  $\text{CH}_2\text{Cl}_2$ :*n*-hexane = 1:4 (v/v) as an eluent and subsequent recrystallization in diethylether:dichloromethane gave orange crystals in a 55%.  $^1\text{H}$  NMR (300 MHz,  $\text{CDCl}_3$ )  $\delta$ : 6.00 (d,  $J$  = 6.0 Hz, 2H), 6.51 (d,  $J$  = 9.0 Hz, 1H), 6.60–6.65 (m, 2H), 6.68–6.76 (m, 4H), 7.29 (dd,  $J$  = 9.0 Hz, 1H), 7.38 (d,  $J$  = 3.0 Hz, 1H), 7.71 (d,  $J$  = 9.0 Hz, 1H), 7.78 (d,  $J$  = 9.0 Hz, 1H).  $^{13}\text{C}\{\text{H}\}$  NMR (126 MHz,  $\text{CDCl}_3$ )  $\delta$ : 29.90, 113.65, 116.06, 117.51, 118.92, 119.47, 122.36, 123.52, 126.80, 130.49, 133.63, 142.79, 144.26, 155.94, 160.16. HR MS (FAB $^+$ , *m*-NBA): calcd for  $\text{C}_{21}\text{H}_{14}\text{NO}_3$  ( $[\text{M}+\text{H}]^+$ ), 327.0895; found, 327.0896. Anal. calcd for  $\text{C}_{21}\text{H}_{13}\text{NO}_2$ : C, 77.05; H, 4.00; N, 4.28. Found: C, 73.85; H, 3.94; N, 4.09.

**Synthesis of PTZC.** PTZC was prepared following the procedures identical to the synthesis of DMACC, except using 10*H*-phenothiazine in place of 9,9-dimethyl-9,10-dihydroacridine. Recrystallization in methanol:chloroform furnished yellow crystals in a 77% yield.  $^1\text{H}$  NMR (300 MHz,  $\text{CDCl}_3$ )  $\delta$ : 6.23 (d,  $J$  = 9.6 Hz, 1H), 6.95 (d,  $J$  = 8.7 Hz, 1H), 6.99 (d,  $J$  = 2.4 Hz, 1H), 7.16–7.22 (m 2H), 7.24–7.33 (m, 5H), 7.42 (d,  $J$  = 7.5 Hz, 2H), 7.61 (d,  $J$  = 4.5 Hz, 1H).  $^{13}\text{C}\{\text{H}\}$  NMR (126 MHz,  $\text{CDCl}_3$ )  $\delta$ : 105.04, 113.37, 113.65, 114.25, 125.60, 126.19, 127.53, 128.85, 128.92, 132.51, 141.41, 143.26, 148.82, 155.77, 161.32. HR MS (FAB $^+$ , *m*-NBA): calcd for  $\text{C}_{21}\text{H}_{14}\text{NO}_2\text{S}$  ( $[\text{M}+\text{H}]^+$ ), 343.0667;

found, 343.0674. Anal. calcd for  $C_{21}H_{13}NO_2S$ : C, 73.45; H, 3.82; N, 4.08; S, 9.34. C, 73.49; H, 3.83; N, 4.08; S, 9.35.

**Cyclic and Differential Pulse Voltammetry.** Cyclic and differential pulse voltammograms of the Ar-saturated  $CH_3CN$  solutions (2.0 mL) containing 2.0 mM sample and 0.10 M TBAPF<sub>6</sub> were collected using a CH instruments, CHI630B instrument at 298 K. Standard three-electrode-assembly consisting of a platinum working electrode, a platinum counter electrode and an Ag/AgNO<sub>3</sub> pseudo reference electrode was used. The potentials were reported against SCE. The ferrocene/ferrocenium redox couple was employed as an external standard. Scan rates for cyclic and differential pulse voltammetries were 0.1 V s<sup>-1</sup> and 4 mV s<sup>-1</sup>, respectively.

**X-ray Crystallography.** Single crystals suitable for X-ray crystallographic analysis were grown by slow diffusion of diethyl ether onto a dichloromethane solution of 0.15 M PTZC at room temperature. A crystal was picked up from the solution and mounted on a Bruker SMART CCD diffractometer equipped with a graphite-monochromated Mo  $K\alpha$  ( $\lambda = 0.71073 \text{ \AA}$ ) radiation source under nitrogen cold stream at 223 K. The CCD data collected and integrated by using a Bruker-SAINT software program. Semi-empirical absorption corrections based on equivalent reflections were applied by Bruker SADABS. Structures were solved and refined using SHELXL97. Hydrogen atoms were placed on the geometrically ideal positions. All non-hydrogen atoms were refined anisotropic thermal parameters. Crystal data for PTZC:  $C_{21}H_{13}NO_2S$ , Monoclinic,  $P2_1/c$ ,  $Z = 8$ ,  $a = 20.4469(7)$ ,  $b = 11.9960(4)$ ,  $c = 13.9932(5) \text{ \AA}$ ,  $\alpha = 90^\circ$ ,  $\beta = 108.3117(12)^\circ$ ,  $\gamma = 90^\circ$ ,  $V = 3258.5(2) \text{ \AA}^3$ ,  $\mu = 0.213 \text{ mm}^{-1}$ ,  $\rho_{\text{calcd}} = 1.400 \text{ Mg/m}^3$ ,  $R_1 = 0.0477$ ,  $wR_2 = 0.1186$  for 8114 unique reflections and 451 variables. The crystallographic data for PTZC are listed in Table S25, which also lists the selected bond distances and angles. CCDC-1941162 for PTZC contains the supplementary crystallographic data for this paper. These data can be obtained free of charge via [www.ccdc.cam.ac.uk/data\\_request/cif](http://www.ccdc.cam.ac.uk/data_request/cif) (or from the Cambridge Crystallographic Data Centre, 12, Union Road, Cambridge CB2 1EZ, UK; fax: (+44) 1223-336-033; or [deposit@ccdc.cam.ac.uk](mailto:deposit@ccdc.cam.ac.uk)).

**Steady-State UV–Vis Absorption and Photoluminescence Measurements.** UV–vis absorption spectra were recorded using a Shimazu, UV-1650 PC spectrometer at 298 K. Photoluminescence spectra were collected on a PTI, Quanta Master 40 scanning

spectrofluorimeter and a Varian, Cary Eclipse fluorescence spectrophotometer. were photoexcited at a wavelength of 350 nm, unless otherwise stated. Solutions were prepared prior to measurements at concentrations of 10 or 50  $\mu\text{M}$ . Variable-temperature experiments were performed using a Peltier or a heating stage. Photoluminescence spectra at cryogenic temperatures were obtained using an Oxford, Optistat DN cryostat. The Lippert–Mataga plot was constructed as a function of solvent polarity parameter ( $f$ );  $f = ((\varepsilon - 1)/(2\varepsilon + 1)) - ((n^2 - 1)/(2n^2 + 1))$  ( $\varepsilon$ , dielectric constant;  $n$ , refractive index).  $f$  values are toluene, 0.0135; chloroform, 0.148; ethyl acetate, 0.200; 2-methyltetrahydrofuran, 0.210; dichloromethane, 0.218; *N,N*-dimethylformamide, 0.275; acetonitrile, 0.305.

**Photoluminescence Lifetime Measurements.** A 50  $\mu\text{M}$  toluene solution was employed for the determination of the photoluminescence lifetime. Photoluminescence decay traces were collected by employing time-correlated single-photon-counting (TCSPC) technique using a Pico Quant, Fluo Time 200 instrument through a motorized monochromator at the peak emission wavelength. 345 nm (PicoQuant, PLS-340) and 377 nm (PicoQuant, LDH375) pulsed lasers were driven by a PDL800-D driver (PicoQuant).

**Determination of Photoluminescence Quantum Yields.** The photoluminescence quantum yield (PLQY) of a sample solution (10  $\mu\text{M}$  in Ar-saturated toluene) was determined relatively by using a 9,10-diphenylanthracene as a standard (toluene, PLQY = 1.00).<sup>[4]</sup> PLQY was calculated according to the following equation:  $\text{PLQY} = \text{PLQY}_{\text{ref}} \times (\text{I/I}_{\text{ref}}) \times (A_{\text{ref}}/A) \times (n/n_{\text{ref}})^2$ , where  $A$ ,  $I$ , and  $n$  are the absorbance at the excitation wavelength, an integrated photoluminescence intensity, and the refractive index of solvent medium, respectively.

**Determination of Exciton Dynamic Parameters Related to TADF.** The rate constants and quantum yields of the exciton dynamic processes of TADF were calculated using the method described previously.<sup>[5,6]</sup> Briefly, the quantum yields for the prompt fluorescence ( $\Phi_{\text{PF}}$ ) and the delayed fluorescence ( $\Phi_{\text{DF}}$ ) were determined using the integrated areas of the prompt and delayed components in the fluorescence decay traces (Fig. S24). The rate constant for radiative decay ( $k_r$ ), internal conversion ( $k_{\text{IC}}$ ), intersystem crossing ( $k_{\text{ISC}}$ ), and reverse intersystem crossing ( $k_{\text{rISC}}$ ) were determined through eqs 1–4:

$$\text{(eq 1)} \quad \Phi_{\text{total}} = \Phi_{\text{PF}} + \Phi_{\text{DF}}$$

$$(eq\ 2)\ k_r = \Phi_{PF}/\tau_{PF}$$

$$(eq\ 3)\ k_{ISC} = \Phi_{DF}/(\tau_{PF} \times \Phi_{total})$$

$$(eq\ 4)\ k_{IC} = (1/\tau_{PF}) - (k_r + k_{ISC})$$

In eqs 1 and 3,  $\Phi_{total}$  is the total photoluminescence quantum yield, and  $\tau_{PF}$  is the lifetime value of the prompt fluorescence. The quantum yields for intersystem crossing ( $\Phi_{ISC}$ ) and ( $\Phi_{rISC}$ ) were calculated using eqs 5 and 6:

$$(eq\ 5)\ \Phi_{ISC} = k_{ISC} \times \tau_{PF}$$

$$(eq\ 6)\ \Phi_{rISC} = (1 - \Phi_{PF}/\Phi_{total})/\Phi_{ISC}$$

Finally, the rate constant for reverse intersystem crossing ( $k_{rISC}$ ) was estimated using eq 7:

$$(eq\ 7)\ k_{rISC} = \Phi_{rISC} \times (\Phi_{total}/\Phi_{PF})/\tau_{DF}$$

**Broadband Femtosecond Transient Absorption Measurements.** A Yb:KGW femtosecond amplifier system (Light Conversion, PHAROS, 400 KHz, 15 W) was used to generate pump and probe pulses. One portion of the amplifier output was directed to non-collinear optical parametric amplifier (Light Conversion, ORPHEUS-N) producing 30-fs pump pulses centred at 700 nm. A beta barium borate crystal was used to tune the pump energy to 350 nm. The pump beam was spectrally filtered with a 425-nm shortpass filter and modulated with an optical chopper at 125 Hz. Another portion of the amplifier was focused onto a YAG crystal and generated white light continuum probe pulses. Two chirp mirrors were used to compensate the positive group velocity dispersion in the probe beam. The pump (2 mJ/cm<sup>2</sup>) and probe beams were spatially overlapped at the sample position. Only the probe beam was sent to a monochromator and detected using an electron-multiplying charge coupled device camera triggered at 250 Hz. The pump-induced changes in the probe transmission were recorded at different pump-probe time delays controlled with a motorized linear stage. The data acquisition was carried out with a LabView software. Typically, 400 excitation pulses were averaged to obtain the transient spectrum at a set delay time. Kinetic traces at appropriate wavelengths were extracted from the time-resolved spectral data. All measurements were performed at room temperature under ambient atmosphere.

**Spectroelectrochemical Measurements.** UV–Vis–NIR absorption spectra of the radical cation species were obtained on an Agilent, Cary 5000 spectrophotometer with

applying anodic potentials (0.50 V to 0.78 V vs Ag<sup>+</sup>/Ag), using the amperometric *I*-*t* curve method. A blank spectrum was taken for a 0.10 M TBAPF<sub>6</sub> solution (CH<sub>3</sub>CN) in an electrochemical cell (beam path length = 0.5 mm) equipped with a Pt mesh working electrode, a Pt wire counter electrode, and a Ag/AgNO<sub>3</sub> pseudo reference electrode.  $\mu$ L of a 2.0 mM DMACC (Ar-saturated acetonitrile containing 0.10 M TBAPF<sub>6</sub> supporting electrolyte) was delivered into the spectroelectrochemical cell.

**DFT/TD-DFT Calculation.** Quantum chemical calculations based on density functional theory (DFT) were performed using a Gaussian 09 program.<sup>[7]</sup> Geometry optimization was conducted at the level of B3LYP and a 6-311+G(d,p) basis set with the conductor-like polarizable continuum model (CPCM) for toluene. Electronic transition energies were calculated using B3LYP, CAM-B3LYP, and PBEh with the same basis sets (6-311+G(d,p)) based on the TD-DFT method.

**Table S1.** Photophysical parameters of thermally activated delayed fluorescence emissions.<sup>a</sup>

	$\Phi_{\text{PF}}$	$\Phi_{\text{DF}}$	$k_{\text{PF}}$ ( $10^7$ , s $^{-1}$ )	$k_{\text{DF}}$ ( $10^3$ , s $^{-1}$ )	$k_{\text{ISC}}$ ( $10^6$ , s $^{-1}$ )	$k_{\text{IC}}$ ( $10^8$ , s $^{-1}$ )	$k_{\text{rISC}}$ ( $10^5$ , s $^{-1}$ )	$\Phi_{\text{ISC}}$	$\Phi_{\text{rISC}}$
spiroACC	0.40	0.0030	8.18	0.14	1.52	1.21	0.46	0.0074	1.00
DMACC	0.15	0.0042	2.44	0.71	4.43	1.34	1.74	0.027	1.00
PXZC	0.17	0.018	2.46	4.00	13.88	1.06	2.46	0.096	1.00
PTZC	0.018	0.023	28.85	20.91	89.90	0.68	20.71	0.56	1.00

<sup>a</sup>50 μM solution in deaerated toluene;  $\Phi_{\text{PF}}$ , the photoluminescence quantum yield of the prompt fluorescence;  $\Phi_{\text{DF}}$ , the photoluminescence quantum yield of the delayed fluorescence;  $\Phi_{\text{ISC}}$ , the quantum yield of intersystem crossing;  $\Phi_{\text{rISC}}$ , the quantum yield of reverse intersystem crossing;  $k_{\text{PF}}$ , the rate constant for the prompt fluorescence;  $k_{\text{DF}}$ , the rate constant for the delayed fluorescence;  $k_{\text{IC}}$ , the rate constant for internal conversion;  $k_{\text{ISC}}$ , the rate constant for intersystem crossing;  $k_{\text{rISC}}$ , the rate constant for reverse intersystem crossing.

**Table S2.** One-electron oxidation and reduction potentials and the driving force for photoinduced intramolecular electron transfer.

	$E_{\text{ox}}$ (V vs SCE) <sup>a</sup>	$E_{\text{red}}$ (V vs. SCE) <sup>a</sup>	$E_{00}$ (eV) <sup>b</sup>	$-\Delta G_{\text{PeT}}$ (eV) <sup>c</sup>
CzC	1.27	-1.66	3.22	0.29
AZPC	1.14	-1.88	3.05	0.03
spiroACC	1.02	-1.62	3.06	0.42
DMACC	0.93	-1.66	2.78	0.19
PXZC	0.75	-1.66	2.56	0.15
PTZC	0.75	-1.65	2.48	0.08

<sup>a</sup>Determined by cyclic and differential pulse voltammetry using CH<sub>3</sub>CN solutions containing 2.0 mM sample and 0.10 M TBAPF<sub>6</sub>. Pt working and counter electrodes and an Ag/AgNO<sub>3</sub> pseudo-reference electrode were employed. <sup>b</sup>The 0–0 transition energy estimated from the onset of the fluorescence spectra. <sup>c</sup>Driving forces for forward electron transfer from the donor to the π–π\* state of coumarin, calculated using the Rehm–Weller equation  $-\Delta G_{\text{PeT}} = -e \cdot [E_{\text{ox}} - E_{\text{red}}] + E_{00}$ .

**Table S3.** Energy levels of the charge-separated species ( $E(\text{CS})$ ), the emissive singlet ICT state ( $E(^1\text{ICT})$ ), and the triplet n– $\pi^*$  transition state ( $E(^3\text{n}-\pi^*)$ ).

	$E(\text{CS})^a$ (eV)	$E(^1\text{ICT})$ (eV)	$E(^3\text{n}-\pi^*)$ (eV)
CzC	2.93	3.22	2.72
AZPC	3.02	3.05	2.58
spiroACC	2.64	3.06	2.73
DMACC	2.59	2.78	2.70
PXZC	2.41	2.56	2.64
PTZC	2.40	2.48	2.53

<sup>a</sup>The energy of charge-separated species (CS) is determined by using equation,  $E(\text{CS}) = e \cdot [E_{\text{ox}}(\text{donor}) - E_{\text{red}}(\text{coumarin})]$ .

**Table S4.** TD-DFT calculation results for the pseudo-equatorial conformers of the dyads obtained with the different functionals.<sup>a</sup>

	B3LYP/6-311+g(d,p)			PBEh/6-311+g(d,p)		
	S <sub>1</sub> (eV)	T <sub>1</sub> (eV)	ΔE <sub>ST</sub> (eV)	S <sub>1</sub> (eV)	T <sub>1</sub> (eV)	ΔE <sub>ST</sub> (eV)
CzC	3.09	2.65	0.44	3.27	2.62	0.65
AZPC	2.05	2.01	0.04	2.23	2.15	0.08
spiroACC	2.55	2.54	0.01	2.75	2.74	0.01
DMACC	2.48	2.47	0.01	2.68	2.66	0.02
PXZC	2.34	2.33	0.01	2.54	2.52	0.02
PTZC	2.57	2.55	0.02	2.78	2.74	0.04

<sup>a</sup>The conductor-like polarizable continuum model (CPCM) for toluene is used.

**Table S5.** TD-DFT calculation results for the pseudo-axial conformers of the dyads obtained with the different functionals.<sup>a</sup>

	B3LYP/6-311+g(d,p)			PBEh/6-311+g(d,p)		
	S <sub>1</sub> (eV)	T <sub>1</sub> (eV)	ΔE <sub>ST</sub> (eV)	S <sub>1</sub> (eV)	T <sub>1</sub> (eV)	ΔE <sub>ST</sub> (eV)
AZPC	3.53	2.58	0.95	3.65	2.55	1.1
spiroACC	3.39	2.57	0.82	3.51	2.53	0.98
DMACC	3.4	2.56	0.84	3.52	2.53	0.99
PXZC	3.46	2.62	0.84	3.59	2.58	1.01
PTZC	3.51	2.62	0.89	3.64	2.58	1.06

<sup>a</sup>The conductor-like polarizable continuum model (CPCM) for toluene is used.

**Table S6.** Report of the Cartesian coordinates of the optimized geometry of CzC.

Center Number	Atomic Number	Atomic Type	Coordinates (Angstroms)		
			X	Y	Z
1	6	0	-3.04003	-0.89083	0.748724
2	6	0	-2.61705	0.054317	-0.18526
3	6	0	-1.27309	0.31296	-0.40541
4	6	0	-0.32724	-0.3734	0.339796
5	6	0	-0.72647	-1.32111	1.290032
6	6	0	-2.06615	-1.57776	1.481618
7	6	0	-4.45749	-1.09394	0.896896
8	6	0	-5.32868	-0.39618	0.153382
9	6	0	-4.87584	0.584127	-0.8222
10	8	0	-3.51393	0.755234	-0.93413
11	8	0	-5.58178	1.250964	-1.5302
12	7	0	1.046342	-0.1103	0.143659
13	6	0	2.027267	-1.06315	-0.13372
14	6	0	3.273449	-0.41854	-0.23937
15	6	0	3.037399	0.991391	-0.01219
16	6	0	1.65749	1.142737	0.217053
17	6	0	1.898014	-2.43395	-0.33626
18	6	0	3.046053	-3.15312	-0.62662
19	6	0	4.294646	-2.5291	-0.72044
20	6	0	4.413565	-1.16277	-0.53251
21	6	0	3.870961	2.106438	0.028271
22	6	0	3.320941	3.347239	0.300152
23	6	0	1.948804	3.479213	0.538884
24	6	0	1.099762	2.385041	0.503519
25	1	0	-0.98325	1.032618	-1.15897
26	1	0	0.022241	-1.83494	1.877785
27	1	0	-2.37936	-2.30818	2.218088
28	1	0	-4.80799	-1.8219	1.61987
29	1	0	-6.39924	-0.51956	0.234301
30	1	0	0.936876	-2.92715	-0.27689
31	1	0	2.97177	-4.22191	-0.78757
32	1	0	5.172151	-3.12136	-0.94835
33	1	0	5.379221	-0.67828	-0.61681
34	1	0	4.935404	2.003364	-0.14686
35	1	0	3.9558	4.223906	0.33373
36	1	0	1.538165	4.45751	0.757823
37	1	0	0.041666	2.500621	0.696821

**Table S7.** Report of the Cartesian coordinates of the optimized geometry of the pseudo-axial conformer of AZPC.

Center Number	Atomic Number	Atomic Type	Coordinates (Angstroms)		
			X	Y	Z
1	6	0	-0.60896	-1.90496	0.362117
2	6	0	-0.32535	-0.51962	0.329313
3	6	0	-1.38612	0.374898	0.154071
4	6	0	-2.67515	-0.10918	0.035985
5	6	0	-2.97356	-1.47255	0.075662
6	6	0	-1.89981	-2.35713	0.238515
7	8	0	-3.6655	0.814911	-0.13079
8	6	0	-4.99462	0.475159	-0.26591
9	6	0	-5.3107	-0.93935	-0.22116
10	6	0	-4.34445	-1.86165	-0.05898
11	8	0	-5.78325	1.374642	-0.40961
12	7	0	0.978191	-0.06947	0.45871
13	6	0	1.301036	1.325689	0.401945
14	6	0	1.97458	1.884987	-0.68755
15	6	0	2.67671	-1.14899	-0.88674
16	6	0	2.082933	-0.97709	0.362803
17	6	0	0.948664	2.115433	1.497225
18	6	0	1.233097	3.467508	1.521998
19	6	0	1.899101	4.040311	0.444359
20	6	0	2.265531	3.251951	-0.631
21	6	0	3.76326	-2.01076	-0.99217
22	6	0	4.240869	-2.68869	0.122596
23	6	0	3.641684	-2.50433	1.361678
24	6	0	2.560754	-1.64097	1.482996
25	6	0	2.442985	1.139475	-1.92487
26	6	0	2.136692	-0.35741	-2.04431
27	1	0	0.196241	-2.61409	0.486478
28	1	0	-1.22761	1.441754	0.104189
29	1	0	-2.09771	-3.42263	0.267752
30	1	0	-6.35509	-1.19548	-0.32629
31	1	0	-4.59361	-2.91696	-0.02911
32	1	0	0.441836	1.643673	2.330434
33	1	0	0.947755	4.067784	2.377084
34	1	0	2.136179	5.097338	0.446055
35	1	0	2.791554	3.702511	-1.46624
36	1	0	4.23798	-2.15405	-1.95662
37	1	0	5.085648	-3.35984	0.023842
38	1	0	4.016803	-3.02719	2.232905
39	1	0	2.08194	-1.47881	2.44122
40	1	0	3.527616	1.273004	-1.99342
41	1	0	2.02477	1.647387	-2.79858
42	1	0	1.057342	-0.51053	-2.12367
43	1	0	2.576014	-0.72042	-2.97534

**Table S8.** Report of the Cartesian coordinates of the optimized geometry of the pseudo-equatorial conformer of AZPC.

Center Number	Atomic Number	Atomic Type	Coordinates (Angstroms)		
			X	Y	Z
1	6	0	-0.77183	-0.75076	1.66548
2	6	0	-0.35531	-0.2204	0.429689
3	6	0	-1.2971	0.13587	-0.53384
4	6	0	-2.65438	-0.03283	-0.25803
5	6	0	-3.09255	-0.56191	0.971821
6	6	0	-2.12188	-0.9181	1.927277
7	8	0	-3.53858	0.326821	-1.23187
8	6	0	-4.9242	0.195899	-1.0834
9	6	0	-5.38134	-0.34446	0.193328
10	6	0	-4.51282	-0.70266	1.165766
11	8	0	-5.62358	0.535434	-2.00662
12	7	0	1.045952	-0.03063	0.159847
13	6	0	1.79982	-1.22958	-0.03934
14	6	0	3.215989	-1.31774	-0.04431
15	6	0	2.624679	1.83345	-0.47111
16	6	0	1.472181	1.33688	0.183195
17	6	0	1.073144	-2.42506	-0.24569
18	6	0	1.69597	-3.66147	-0.367
19	6	0	3.08299	-3.75547	-0.3122
20	6	0	3.811806	-2.57919	-0.17576
21	6	0	2.883221	3.209384	-0.43417
22	6	0	2.053063	4.11585	0.217157
23	6	0	0.941343	3.622087	0.893729
24	6	0	0.665264	2.259701	0.88404
25	6	0	4.126697	-0.11606	-0.0489
26	6	0	3.657377	0.928859	-1.08546
27	1	0	-0.02367	-1.02451	2.400981
28	1	0	-0.99041	0.545358	-1.48914
29	1	0	-2.44717	-1.32179	2.881911
30	1	0	-6.45489	-0.43716	0.303434
31	1	0	-4.87381	-1.10408	2.10939
32	1	0	-0.00466	-2.39029	-0.31794
33	1	0	1.084504	-4.54656	-0.51614
34	1	0	3.58729	-4.71222	-0.40142
35	1	0	4.898004	-2.62268	-0.17904
36	1	0	3.776046	3.568856	-0.93939
37	1	0	2.280799	5.176931	0.210591
38	1	0	0.284198	4.290286	1.442388
39	1	0	-0.19744	1.906556	1.432575
40	1	0	4.184586	0.364363	0.935607
41	1	0	5.139362	-0.4554	-0.28848
42	1	0	3.276429	0.407201	-1.97188
43	1	0	4.503632	1.537781	-1.4182

**Table S9.** Report of the Cartesian coordinates of the optimized geometry of the pseudo-axial conformer of spiroACC.

Center Number	Atomic Number	Atomic Type	Coordinates (Angstroms)		
			X	Y	Z
1	6	0	2.263903	1.734656	-0.98025
2	6	0	1.833824	1.047689	0.178413
3	6	0	2.706244	0.111541	0.741013
4	6	0	3.956927	-0.09099	0.186663
5	6	0	4.401937	0.598858	-0.93956
6	6	0	3.511256	1.512428	-1.51253
7	8	0	4.752036	-1.01693	0.796765
8	6	0	6.021109	-1.32215	0.354077
9	6	0	6.491566	-0.60334	-0.81608
10	6	0	5.717425	0.309286	-1.42884
11	8	0	6.636452	-2.1553	0.968059
12	7	0	0.556596	1.262964	0.712918
13	6	0	0.004254	0.402972	1.708557
14	6	0	-1.19828	-0.25043	1.435173
15	6	0	-1.63631	1.472242	-0.30597
16	6	0	-0.41615	2.056259	0.035902
17	6	0	0.613759	0.268557	2.952818
18	6	0	0.081481	-0.58907	3.900735
19	6	0	-1.07795	-1.2969	3.614661
20	6	0	-1.71791	-1.11023	2.39945
21	6	0	-2.57095	2.245605	-0.99027
22	6	0	-2.31467	3.571255	-1.30332
23	6	0	-1.12376	4.15924	-0.89835
24	6	0	-0.18222	3.404751	-0.2193
25	6	0	-1.92119	0.025565	0.11245
26	6	0	-3.42047	-0.23712	0.227674
27	6	0	-3.82725	-1.23249	-0.66016
28	6	0	-2.65565	-1.69644	-1.41197
29	6	0	-1.53168	-0.98268	-0.98289
30	6	0	-2.54839	-2.66698	-2.39828
31	6	0	-1.30146	-2.92096	-2.95552
32	6	0	-0.183	-2.21276	-2.52888
33	6	0	-0.29135	-1.23901	-1.53958
34	6	0	-4.33636	0.375111	1.065587
35	6	0	-5.66909	-0.01779	1.007642
36	6	0	-6.07615	-1.01192	0.120542
37	6	0	-5.15844	-1.62726	-0.72029
38	1	0	1.606954	2.429625	-1.47658
39	1	0	2.436863	-0.48673	1.595823
40	1	0	3.81097	2.051473	-2.40394
41	1	0	7.487687	-0.85042	-1.15401
42	1	0	6.078858	0.83806	-2.30405
43	1	0	1.503954	0.842912	3.173836
44	1	0	0.566903	-0.69526	4.863049
45	1	0	-1.4986	-1.97604	4.345912
46	1	0	-2.64291	-1.63497	2.199401
47	1	0	-3.51822	1.805641	-1.27336
48	1	0	-3.05552	4.150358	-1.84071

49	1	0	-0.93159	5.205929	-1.09998
50	1	0	0.74098	3.856181	0.120427
51	1	0	-3.41969	-3.21984	-2.72967
52	1	0	-1.19875	-3.6759	-3.72574
53	1	0	0.784978	-2.42089	-2.96867
54	1	0	0.591991	-0.70209	-1.22127
55	1	0	-4.02488	1.148854	1.757872
56	1	0	-6.39694	0.452731	1.657643
57	1	0	-7.11816	-1.30697	0.087539
58	1	0	-5.47892	-2.40062	-1.4085

**Table S10.** Report of the Cartesian coordinates of the optimized geometry of the pseudo-equatorial conformer of spiroACC.

Center Number	Atomic Number	Atomic Type	Coordinates (Angstroms)		
			X	Y	Z
1	6	0	-2.72729	-1.87468	0.000583
2	6	0	-2.23926	-0.56585	0.000139
3	6	0	-3.10809	0.510088	-0.00024
4	6	0	-4.47448	0.2686	-0.00021
5	6	0	-4.98666	-1.0282	0.000244
6	6	0	-4.08754	-2.10019	0.000654
7	8	0	-5.29926	1.353737	-0.00068
8	6	0	-6.67093	1.247766	-0.00109
9	6	0	-7.21837	-0.10194	0.000092
10	6	0	-6.42017	-1.17863	0.000457
11	8	0	-7.31104	2.264687	-7.6E-05
12	7	0	-0.82854	-0.33566	0.000084
13	6	0	-0.14952	-0.25076	-1.22356
14	6	0	1.236718	-0.07449	-1.26374
15	6	0	1.236682	-0.07362	1.263785
16	6	0	-0.14956	-0.24991	1.223685
17	6	0	-0.86162	-0.34031	-2.42945
18	6	0	-0.21183	-0.25657	-3.64554
19	6	0	1.165602	-0.08056	-3.69281
20	6	0	1.866268	0.007647	-2.5045
21	6	0	1.866197	0.009373	2.504505
22	6	0	1.165497	-0.07801	3.69286
23	6	0	-0.21194	-0.25405	3.645673
24	6	0	-0.86169	-0.33863	2.429621
25	6	0	2.084193	0.029262	0.000001
26	6	0	2.913086	1.317396	-0.00043
27	6	0	4.280896	1.03461	-0.00033
28	6	0	4.457096	-0.42463	0.00018
29	6	0	3.195975	-1.02492	0.000383
30	6	0	5.608609	-1.20184	0.00046
31	6	0	5.481155	-2.5853	0.000946
32	6	0	4.222428	-3.18164	0.001148
33	6	0	3.070137	-2.40197	0.000866
34	6	0	2.463071	2.624941	-0.00089
35	6	0	3.396845	3.656283	-0.00124
36	6	0	4.761365	3.376672	-0.00113
37	6	0	5.214506	2.063342	-0.00068
38	1	0	-2.02686	-2.69985	0.000897
39	1	0	-2.73845	1.527057	-0.0006
40	1	0	-4.47488	-3.11207	0.00105
41	1	0	-8.29687	-0.17156	0.000523
42	1	0	-6.83966	-2.17825	0.001067
43	1	0	-1.93348	-0.47508	-2.41153
44	1	0	-0.78794	-0.32825	-4.56033
45	1	0	1.684054	-0.01282	-4.64079
46	1	0	2.941115	0.144935	-2.52979
47	1	0	2.941078	0.146678	2.529736
48	1	0	1.683922	-0.00963	4.640808

49	1	0	-0.78807	-0.32511	4.56049
50	1	0	-1.93355	-0.47342	2.411763
51	1	0	6.590485	-0.74288	0.000307
52	1	0	6.368614	-3.20692	0.001171
53	1	0	4.141016	-4.26207	0.001526
54	1	0	2.092201	-2.87013	0.001023
55	1	0	1.401844	2.846861	-0.00097
56	1	0	3.060514	4.686229	-0.0016
57	1	0	5.475323	4.191676	-0.00141
58	1	0	6.277414	1.851148	-0.0006

**Table S11.** Report of the Cartesian coordinates of the optimized geometry of the pseudo-axial conformer of DMACC.

Center Number	Atomic Number	Atomic Type	Coordinates (Angstroms)		
			X	Y	Z
1	6	0	0.925204	-1.93822	-0.16952
2	6	0	0.592549	-0.5826	-0.39471
3	6	0	1.615243	0.366429	-0.30892
4	6	0	2.910758	-0.03726	-0.044
5	6	0	3.256892	-1.37302	0.156069
6	6	0	2.220809	-2.31158	0.094516
7	8	0	3.856421	0.944501	0.01839
8	6	0	5.186728	0.688692	0.271844
9	6	0	5.553515	-0.70029	0.476852
10	6	0	4.631203	-1.67755	0.421958
11	8	0	5.935492	1.631518	0.303368
12	7	0	-0.72459	-0.2008	-0.65571
13	6	0	-1.13708	1.166476	-0.65006
14	6	0	-2.13028	1.539654	0.259844
15	6	0	-2.83183	-0.80448	0.363789
16	6	0	-1.81888	-1.11154	-0.54908
17	6	0	-0.63779	2.072291	-1.57753
18	6	0	-1.08553	3.384566	-1.57329
19	6	0	-2.05411	3.77731	-0.66154
20	6	0	-2.57968	2.856119	0.235293
21	6	0	-3.93015	-1.65598	0.433852
22	6	0	-4.01831	-2.78191	-0.37456
23	6	0	-3.01571	-3.05865	-1.29238
24	6	0	-1.92165	-2.21256	-1.39018
25	6	0	-2.67245	0.46447	1.204233
26	6	0	-3.9889	0.886935	1.857243
27	6	0	-1.64461	0.2077	2.330918
28	1	0	0.15746	-2.69497	-0.18608
29	1	0	1.430618	1.421846	-0.4296
30	1	0	2.447897	-3.35761	0.265997
31	1	0	6.598697	-0.88972	0.674769
32	1	0	4.917055	-2.71184	0.579765
33	1	0	0.090909	1.743896	-2.30768
34	1	0	-0.69003	4.090932	-2.29275
35	1	0	-2.41555	4.798413	-0.65636
36	1	0	-3.35249	3.177052	0.920371
37	1	0	-4.73589	-1.44459	1.123652
38	1	0	-4.88124	-3.43212	-0.29741
39	1	0	-3.09172	-3.91936	-1.94548
40	1	0	-1.14941	-2.39558	-2.12658
41	1	0	-4.76773	1.08918	1.119394
42	1	0	-4.34655	0.108623	2.532235
43	1	0	-3.84471	1.783456	2.461124
44	1	0	-2.00859	-0.57982	2.994581
45	1	0	-0.67374	-0.09738	1.942764
46	1	0	-1.50407	1.116991	2.919365

**Table S12.** Report of the Cartesian coordinates of the optimized geometry of the pseudo-equatorial conformer of DMACC.

Center Number	Atomic Number	Atomic Type	Coordinates (Angstroms)		
			X	Y	Z
1	6	0	-1.18451	-2E-06	1.822549
2	6	0	-0.74002	-1.7E-05	0.498085
3	6	0	-1.64475	-1.9E-05	-0.54795
4	6	0	-3.00231	-1.9E-05	-0.26111
5	6	0	-3.4711	-1.2E-05	1.051987
6	6	0	-2.53645	-1E-06	2.093323
7	8	0	-3.86275	-2.8E-05	-1.31831
8	6	0	-5.23015	-3.8E-05	-1.16696
9	6	0	-5.7324	-1.5E-05	0.20004
10	6	0	-4.89878	-8E-06	1.249702
11	8	0	-5.90345	-1.7E-05	-2.16235
12	7	0	0.661456	-1.2E-05	0.219385
13	6	0	1.33641	-1.22463	0.111507
14	6	0	2.715072	-1.26161	-0.13313
15	6	0	2.715033	1.261645	-0.13313
16	6	0	1.336373	1.224624	0.111505
17	6	0	0.625998	-2.42537	0.247228
18	6	0	1.265202	-3.64681	0.143097
19	6	0	2.629676	-3.69783	-0.10013
20	6	0	3.327966	-2.5094	-0.23408
21	6	0	3.327882	2.509459	-0.23407
22	6	0	2.629546	3.697863	-0.10013
23	6	0	1.265073	3.646795	0.143091
24	6	0	0.625914	2.42533	0.247221
25	6	0	3.559348	0.00003	-0.30021
26	6	0	4.188137	0.000033	-1.70979
27	6	0	4.681801	0.000041	0.758938
28	1	0	-0.45705	0.000007	2.623998
29	1	0	-1.30897	-2.5E-05	-1.5766
30	1	0	-2.8896	0.000009	3.11769
31	1	0	-6.80799	-7E-06	0.305508
32	1	0	-5.28533	0.000004	2.262534
33	1	0	-0.43776	-2.40202	0.434611
34	1	0	0.690057	-4.55855	0.251759
35	1	0	3.143887	-4.64682	-0.1859
36	1	0	4.392776	-2.55447	-0.42663
37	1	0	4.39269	2.554566	-0.42662
38	1	0	3.143723	4.646871	-0.1859
39	1	0	0.689893	4.558506	0.251751
40	1	0	-0.43784	2.401936	0.4346
41	1	0	3.412581	0.000037	-2.47802
42	1	0	4.81397	0.881607	-1.85817
43	1	0	4.813966	-0.88154	-1.85818
44	1	0	5.317731	0.880498	0.65563
45	1	0	4.261269	0.000046	1.766365
46	1	0	5.317736	-0.88042	0.655641

**Table S13.** Report of the Cartesian coordinates of the optimized geometry of the pseudo-axial conformer of PXZC.

Center Number	Atomic Number	Atomic Type	Coordinates (Angstroms)		
			X	Y	Z
1	6	0	-0.55687	-1.91523	0.214027
2	6	0	-0.27542	-0.54228	0.373458
3	6	0	-1.32979	0.366068	0.280004
4	6	0	-2.61459	-0.09364	0.05332
5	6	0	-2.91172	-1.44758	-0.09339
6	6	0	-1.84253	-2.34599	-0.01257
7	8	0	-3.59699	0.84934	-0.0254
8	6	0	-4.92022	0.535643	-0.24869
9	6	0	-5.23691	-0.87311	-0.4002
10	6	0	-4.27857	-1.81278	-0.32587
11	8	0	-5.70473	1.447382	-0.30019
12	7	0	1.035996	-0.10028	0.625099
13	6	0	1.377975	1.275021	0.44511
14	6	0	2.223642	1.584314	-0.61506
15	6	0	2.983279	-0.60025	-0.69552
16	6	0	2.151434	-0.95304	0.362402
17	6	0	0.944369	2.292759	1.283882
18	6	0	1.291512	3.6088	1.012184
19	6	0	2.096538	3.907215	-0.081
20	6	0	2.582108	2.891391	-0.89181
21	6	0	4.06952	-1.38126	-1.04789
22	6	0	4.338639	-2.52867	-0.31577
23	6	0	3.547972	-2.86541	0.77677
24	6	0	2.464693	-2.07044	1.124723
25	8	0	2.743284	0.566941	-1.3849
26	1	0	0.238469	-2.64221	0.254274
27	1	0	-1.18127	1.43079	0.365992
28	1	0	-2.03503	-3.40547	-0.13627
29	1	0	-6.27702	-1.10794	-0.57501
30	1	0	-4.52752	-2.86187	-0.44285
31	1	0	0.323968	2.049383	2.13716
32	1	0	0.935543	4.401256	1.658049
33	1	0	2.366434	4.934376	-0.29214
34	1	0	3.238898	3.093912	-1.72815
35	1	0	4.691601	-1.07686	-1.87989
36	1	0	5.183979	-3.14902	-0.58616
37	1	0	3.778001	-3.74523	1.36416
38	1	0	1.849138	-2.31775	1.980398

**Table S14.** Report of the Cartesian coordinates of the optimized geometry of the pseudo-equatorial conformer of PXZC.

Center Number	Atomic Number	Atomic Type	Coordinates (Angstroms)		
			X	Y	Z
1	6	0	-0.71308	-0.00013	1.678784
2	6	0	-0.35693	-3.9E-05	0.326624
3	6	0	-1.32629	0.000022	-0.65844
4	6	0	-2.6631	-9E-06	-0.28334
5	6	0	-3.04463	-0.0001	1.057139
6	6	0	-2.04411	-0.00016	2.036094
7	8	0	-3.5897	0.000056	-1.28225
8	6	0	-4.94495	0.00005	-1.04255
9	6	0	-5.35668	-5.8E-05	0.354439
10	6	0	-4.4567	-0.00013	1.347562
11	8	0	-5.68113	0.000138	-1.99193
12	7	0	1.019517	-4E-06	-0.05343
13	6	0	1.740785	-1.2083	-0.04056
14	6	0	3.109523	-1.17785	-0.32301
15	6	0	3.109476	1.177931	-0.32297
16	6	0	1.740739	1.208315	-0.04051
17	6	0	1.151384	-2.44056	0.220239
18	6	0	1.90741	-3.60837	0.197513
19	6	0	3.263221	-3.55989	-0.07653
20	6	0	3.86401	-2.33208	-0.33428
21	6	0	3.86392	2.332191	-0.33419
22	6	0	3.263086	3.559969	-0.07639
23	6	0	1.907273	3.608381	0.19765
24	6	0	1.151292	2.440548	0.220337
25	8	0	3.746858	0.000059	-0.64193
26	1	0	0.063477	-0.00018	2.432955
27	1	0	-1.05598	0.000093	-1.706
28	1	0	-2.32981	-0.00023	3.08126
29	1	0	-6.4231	-7.1E-05	0.5299
30	1	0	-4.77713	-0.0002	2.383213
31	1	0	0.092572	-2.49082	0.434264
32	1	0	1.422591	-4.55578	0.3972
33	1	0	3.856353	-4.46516	-0.09403
34	1	0	4.920628	-2.25355	-0.55777
35	1	0	4.92054	2.253712	-0.55769
36	1	0	3.856184	4.465261	-0.09386
37	1	0	1.422419	4.555774	0.397377
38	1	0	0.09248	2.490757	0.434371

**Table S15.** Report of the Cartesian coordinates of the optimized geometry of the pseudo-axial conformer of PTZC.

Center Number	Atomic Number	Atomic Type	Coordinates (Angstroms)		
			X	Y	Z
1	6	0	0.645653	-1.92601	-0.18751
2	6	0	0.371151	-0.55239	-0.36016
3	6	0	1.42986	0.35367	-0.28066
4	6	0	2.712816	-0.11047	-0.05583
5	6	0	3.004021	-1.46505	0.103582
6	6	0	1.930186	-2.35992	0.036606
7	8	0	3.701391	0.82776	0.007466
8	6	0	5.024218	0.508638	0.225255
9	6	0	5.334044	-0.89946	0.391185
10	6	0	4.369549	-1.83449	0.332618
11	8	0	5.814269	1.416914	0.260659
12	7	0	-0.9339	-0.10939	-0.6034
13	6	0	-1.2609	1.27784	-0.51085
14	6	0	-2.00439	1.720155	0.581592
15	16	0	-2.54924	0.530497	1.785876
16	6	0	-2.8843	-0.80787	0.664364
17	6	0	-2.04791	-0.98678	-0.43609
18	6	0	-3.97248	-1.65107	0.859498
19	6	0	-4.21913	-2.67556	-0.04203
20	6	0	-3.40641	-2.83507	-1.15835
21	6	0	-2.33296	-1.98137	-1.36347
22	6	0	-0.88495	2.178645	-1.49942
23	6	0	-1.19274	3.524182	-1.36525
24	6	0	-1.90662	3.967798	-0.25828
25	6	0	-2.33068	3.065784	0.705913
26	1	0	-0.15664	-2.64693	-0.21918
27	1	0	1.281865	1.417912	-0.38027
28	1	0	2.119352	-3.41891	0.169876
29	1	0	6.373831	-1.13808	0.56259
30	1	0	4.613412	-2.88363	0.459846
31	1	0	-4.62639	-1.49747	1.709107
32	1	0	-5.06321	-3.3356	0.115264
33	1	0	-3.61537	-3.6183	-1.87627
34	1	0	-1.69843	-2.08674	-2.2348
35	1	0	-0.33835	1.817815	-2.36191
36	1	0	-0.88305	4.225263	-2.13007
37	1	0	-2.15458	5.016992	-0.15582
38	1	0	-2.9208	3.400778	1.550033

**Table S16.** Report of the Cartesian coordinates of the optimized geometry of the pseudo-equatorial conformer of PTZC.

Center Number	Atomic Number	Atomic Type	Coordinates (Angstroms)		
			X	Y	Z
1	6	0	0.872871	-0.00003	1.895684
2	6	0	0.461875	-1.5E-05	0.561633
3	6	0	1.397284	0	-0.46046
4	6	0	2.745682	-5E-06	-0.13722
5	6	0	3.17981	-2.4E-05	1.188005
6	6	0	2.217933	-3.6E-05	2.202735
7	8	0	3.63364	0.000009	-1.17182
8	6	0	4.996787	0.000011	-0.98433
9	6	0	5.462789	-1.9E-05	0.395569
10	6	0	4.602122	-3.2E-05	1.42303
11	8	0	5.695767	0.000005	-1.9617
12	7	0	-0.9419	-6E-06	0.280693
13	6	0	-1.56402	1.229988	-0.04507
14	6	0	-2.95695	1.344794	0.023668
15	16	0	-3.91682	0.000022	0.665101
16	6	0	-2.95697	-1.34477	0.023658
17	6	0	-1.56404	-1.22999	-0.04508
18	6	0	-3.58909	-2.53154	-0.31885
19	6	0	-2.84635	-3.6449	-0.68494
20	6	0	-1.46441	-3.55022	-0.72473
21	6	0	-0.82851	-2.35379	-0.42208
22	6	0	-0.82846	2.353773	-0.42207
23	6	0	-1.46433	3.550219	-0.7247
24	6	0	-2.84628	3.644931	-0.68491
25	6	0	-3.58904	2.531584	-0.31883
26	1	0	0.122669	-3.9E-05	2.675446
27	1	0	1.096555	0.000017	-1.50014
28	1	0	2.542112	-0.00005	3.236606
29	1	0	6.535266	-2.8E-05	0.529088
30	1	0	4.962197	-4.9E-05	2.445546
31	1	0	-4.67042	-2.58356	-0.27595
32	1	0	-3.345	-4.57315	-0.93316
33	1	0	-0.86605	-4.4087	-1.00431
34	1	0	0.249419	-2.3034	-0.47119
35	1	0	0.249467	2.303356	-0.47118
36	1	0	-0.86596	4.408693	-1.00429
37	1	0	-3.34491	4.573195	-0.93313
38	1	0	-4.67037	2.583624	-0.27593

**Table S17.** Summary of the TD-B3LYP calculation results for CzC.

state	energy (eV)	participating molecular orbitals (expansion coefficient)
T <sub>1</sub>	2.65	HOMO → LUMO (0.65), HOMO-2 → LUMO (0.24)
S <sub>1</sub>	3.09	HOMO → LUMO (0.99)
T <sub>2</sub>	3.22	HOMO-1 → LUMO+1 (0.69)
T <sub>3</sub>	3.27	HOMO-2 → LUMO (0.52)
T <sub>4</sub>	3.37	HOMO → LUMO+1 (0.83)

**Table S18.** Summary of the TD-B3LYP calculation results for the pseudo-axial conformer of AZPC.

state	energy (eV)	participating molecular orbitals (expansion coefficient)
T <sub>1</sub>	2.58	HOMO → LUMO (0.90)
S <sub>1</sub>	3.53	HOMO → LUMO (0.97)
T <sub>2</sub>	3.61	HOMO → LUMO+1 (0.18)
T <sub>3</sub>	3.72	HOMO-1 → LUMO (0.40)

**Table S19.** Summary of the TD-B3LYP calculation results for the pseudo-equatorial conformer of AZPC.

state	energy (eV)	participating molecular orbitals (expansion coefficient)
T <sub>1</sub>	2.01	HOMO → LUMO (0.96)
S <sub>1</sub>	2.05	HOMO → LUMO (0.99)
T <sub>2</sub>	2.40	HOMO-2 → LUMO (0.60)
T <sub>3</sub>	3.07	HOMO → LUMO+3 (0.69)
T <sub>4</sub>	3.10	HOMO-5 → LUMO (0.59)

**Table S20.** Summary of the TD-B3LYP calculation results for the pseudo-axial conformer of spiroACC.

state	energy (eV)	participating molecular orbitals (expansion coefficient)
T <sub>1</sub>	2.57	HOMO → LUMO (0.86)
T <sub>2</sub>	3.11	HOMO-1 → LUMO+1 (0.69)
S <sub>1</sub>	3.39	HOMO → LUMO (0.98)
T <sub>3</sub>	3.52	HOMO → LUMO+4 (0.28), HOMO-3 → LUMO (0.19)

**Table S21.** Summary of the TD-B3LYP calculation results for the pseudo-equatorial conformer of spiroACC.

state	energy (eV)	participating molecular orbitals (expansion coefficient)
T <sub>1</sub>	2.54	HOMO → LUMO (0.98)
S <sub>1</sub>	2.55	HOMO → LUMO (0.99)
T <sub>2</sub>	2.87	HOMO-4 → LUMO (0.64)
T <sub>3</sub>	3.12	HOMO-1 → LUMO+1 (0.67)

**Table S22.** Summary of the TD-B3LYP calculation results for the pseudo-axial conformer of DMACC.

state	energy (eV)	participating molecular orbitals (expansion coefficient)
T <sub>1</sub>	2.56	HOMO → LUMO (0.87)
S <sub>1</sub>	3.40	HOMO → LUMO (0.98)
T <sub>2</sub>	3.53	HOMO-1 → LUMO (0.18), HOMO → LUMO+1 (0.24)
T <sub>3</sub>	3.62	HOMO → LUMO+3 (0.19)
T <sub>4</sub>	3.75	HOMO-1 → LUMO (0.46)

**Table S23.** Summary of the TD-B3LYP calculation results for the pseudo-equatorial conformer of DMACC.

state	energy (eV)	participating molecular orbitals (expansion coefficient)
T <sub>1</sub>	2.47	HOMO → LUMO (0.98)
S <sub>1</sub>	2.48	HOMO → LUMO (0.99)
T <sub>2</sub>	2.87	HOMO-2 → LUMO (0.32), HOMO-3 → LUMO (0.34)
T <sub>3</sub>	3.24	HOMO → LUMO+4 (0.64)
T <sub>4</sub>	3.53	HOMO → LUMO+3 (0.94)

**Table S24.** Summary of the TD-B3LYP calculation results for the pseudo-axial conformer of PXZC.

state	energy (eV)	participating molecular orbitals (expansion coefficient)
T <sub>1</sub>	2.62	HOMO → LUMO (0.80)
S <sub>1</sub>	3.46	HOMO → LUMO (0.97)
T <sub>2</sub>	3.57	HOMO → LUMO+1 (0.33)
T <sub>3</sub>	3.59	HOMO → LUMO+2 (0.28), HOMO → LUMO+3 (0.19)
T <sub>4</sub>	3.72	HOMO-2 → LUMO (0.41)

**Table S25.** Summary of the TD-B3LYP calculation results for the pseudo-equatorial conformer of PXZC.

state	energy (eV)	participating molecular orbitals (expansion coefficient)
T <sub>1</sub>	2.33	HOMO → LUMO (0.98)
S <sub>1</sub>	2.34	HOMO → LUMO (0.99)
T <sub>2</sub>	2.88	HOMO-2 → LUMO (0.73)
T <sub>3</sub>	2.95	HOMO → LUMO+3 (0.45)
T <sub>4</sub>	3.36	HOMO → LUMO+1 (0.53)

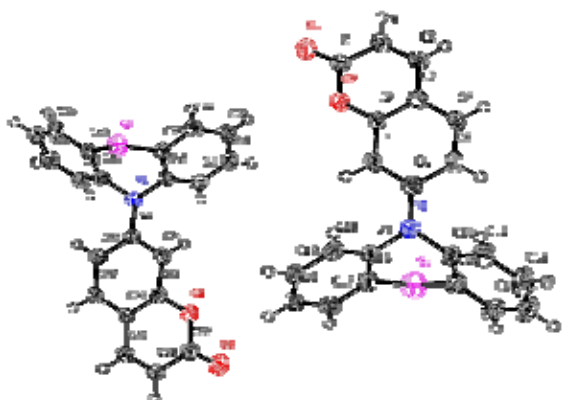
**Table S26.** Summary of the TD-B3LYP Calculation Results for the pseudo-axial conformer of PTZC.

state	energy (eV)	participating molecular orbitals (expansion coefficient)
T <sub>1</sub>	2.62	HOMO → LUMO (0.82)
T <sub>2</sub>	3.49	HOMO → LUMO+1 (0.13), HOMO → LUMO+3 (0.15)
S <sub>1</sub>	3.51	HOMO → LUMO (0.97)
T <sub>3</sub>	3.55	HOMO-1 → LUMO+2 (0.24), HOMO → LUMO+4 (0.17)
T <sub>4</sub>	3.73	HOMO-2 → LUMO (0.60)

**Table S27.** Summary of the TD-B3LYP calculation results for the pseudo-equatorial conformer of PTZC.

state	energy (eV)	participating molecular orbitals (expansion coefficient)
T <sub>1</sub>	2.55	HOMO → LUMO (0.97)
S <sub>1</sub>	2.57	HOMO → LUMO (0.98)
T <sub>2</sub>	2.87	HOMO-2 → LUMO (0.72)
T <sub>3</sub>	3.11	HOMO → LUMO+1 (0.36), HOMO → LUMO+2 (0.34)
T <sub>4</sub>	3.47	HOMO → LUMO+3 (0.68)

**Table S28.** Crystallographic data and selected bond distances ( $\text{\AA}$ ) and angles ( $^\circ$ ) of PTZC.



Crystal Data	
Chemical formula	$\text{C}_{21}\text{H}_{13}\text{NO}_2\text{S}$
Molecular weight	343.38
Crystal system	monoclinic
$a/\text{\AA}$	20.4469(7)
$b/\text{\AA}$	11.9960(7)
$c/\text{\AA}$	13.9932(5)
$\alpha/^\circ$	90.00
$\beta/^\circ$	108.3117(12)
$\gamma/^\circ$	90.00
Unit cell volume/ $\text{\AA}^3$	3258.5(2)
Temperature/K	223(2)
Space group	$\text{P}2_1/c$
No. of formula units per unit cell, Z	8
Radiation type	Mo K $\alpha$
Absorption coefficient, $\mu/\text{mm}^{-1}$	0.213
Calculated density, $\rho_{\text{calcd}}/\text{Mg m}^{-3}$	1.400
$R$ value	0.0477
wR <sub>2</sub> value	0.1186

Bond Length ( $\text{\AA}$ )					
O(1)-C(1)	1.204(2)	C(14)-C(15)	1.388(3)	C(28)-C(29)	1.427(3)
C(1)-O(2)	1.384(2)	C(14)-H(14)	0.94	C(29)-C(30)	1.334(3)
C(1)-C(9)	1.442(3)	C(15)-S(1)	1.763(2)	C(29)-H(29)	0.94
O(2)-C(2)	1.376(2)	S(1)-C(16)	1.769(2)	C(30)-H(30)	0.94
C(2)-C(3)	1.374(3)	C(16)-C(21)	1.388(3)	N(2)-C(42)	1.431(2)
C(2)-C(7)	1.393(3)	C(16)-C(17)	1.388(3)	N(2)-C(31)	1.435(2)
C(3)-C(4)	1.392(3)	C(17)-C(18)	1.377(3)	C(31)-C(36)	1.387(3)
C(3)-H(3)	0.94	C(17)-H(17)	0.94	C(31)-C(32)	1.389(3)
C(4)-N(1)	1.397(2)	C(18)-C(19)	1.386(3)	C(32)-C(33)	1.381(3)
C(4)-C(5)	1.410(3)	C(18)-H(18)	0.94	C(32)-H(32)	0.94
C(5)-C(6)	1.366(3)	C(19)-C(20)	1.387(3)	C(33)-C(34)	1.379(3)
C(5)-H(5)	0.94	C(19)-H(19)	0.94	C(33)-H(33)	0.94
C(6)-C(7)	1.397(3)	C(20)-C(21)	1.382(3)	C(34)-C(35)	1.379(3)
C(6)-H(6)	0.94	C(20)-H(20)	0.94	C(34)-H(34)	0.94
C(7)-C(8)	1.424(3)	O(3)-C(22)	1.202(3)	C(35)-C(36)	1.385(3)
C(8)-C(9)	1.336(3)	C(22)-O(4)	1.389(2)	C(35)-H(35)	0.94
C(8)-H(8)	0.94	C(22)-C(30)	1.437(3)	C(36)-S(2)	1.7670(19)
C(9)-H(9)	0.94	O(4)-C(23)	1.377(2)	S(2)-C(37)	1.7664(19)
N(1)-C(10)	1.435(2)	C(23)-C(24)	1.375(3)	C(37)-C(42)	1.388(3)
N(1)-C(21)	1.438(2)	C(23)-C(28)	1.397(3)	C(37)-C(38)	1.393(3)

C(10)-C(11)	1.386(3)	C(24)-C(25)	1.391(3)	C(38)-C(39)	1.378(3)
C(10)-C(15)	1.387(3)	C(24)-H(24)	0.94	C(38)-H(38)	0.94
C(11)-C(12)	1.381(3)	C(25)-N(2)	1.397(2)	C(39)-C(40)	1.379(3)
C(11)-H(11)	0.94	C(25)-C(26)	1.409(3)	C(39)-H(39)	0.94
C(12)-C(13)	1.374(4)	C(26)-C(27)	1.370(3)	C(40)-C(41)	1.381(3)
C(12)-H(12)	0.94	C(26)-H(26)	0.94	C(40)-H(40)	0.94
C(13)-C(14)	1.379(3)	C(27)-C(28)	1.394(3)	C(41)-C(42)	1.384(3)
C(13)-H(13)	0.94	C(27)-H(27)	0.94	C(41)-H(41)	0.94
Bond Angle (°)					
O(1)-C(1)-O(2)	116.66(17)	C(10)-C(15)-C(14)	119.7(2)	C(28)-C(29)-H(29)	119.5
O(1)-C(1)-C(9)	126.94(19)	C(10)-C(15)-S(1)	119.17(15)	C(29)-C(30)-C(22)	121.59(19)
O(2)-C(1)-C(9)	116.39(18)	C(14)-C(15)-S(1)	121.11(17)	C(29)-C(30)-H(30)	119.2
C(2)-O(2)-C(1)	122.61(15)	C(15)-S(1)-C(16)	97.75(9)	C(22)-C(30)-H(30)	119.2
C(3)-C(2)-O(2)	116.85(16)	C(21)-C(16)-C(17)	119.96(18)	C(25)-N(2)-C(42)	120.47(15)
C(3)-C(2)-C(7)	122.90(18)	C(21)-C(16)-S(1)	119.01(15)	C(25)-N(2)-C(31)	120.61(15)
O(2)-C(2)-C(7)	120.23(17)	C(17)-C(16)-S(1)	121.02(16)	C(42)-N(2)-C(31)	114.08(15)
C(2)-C(3)-C(4)	119.76(17)	C(18)-C(17)-C(16)	119.84(19)	C(36)-C(31)-C(32)	119.79(18)
C(2)-C(3)-H(3)	120.1	C(18)-C(17)-H(17)	120.1	C(36)-C(31)-N(2)	118.97(16)
C(4)-C(3)-H(3)	120.1	C(16)-C(17)-H(17)	120.1	C(32)-C(31)-N(2)	121.18(17)
C(3)-C(4)-N(1)	121.68(16)	C(17)-C(18)-C(19)	120.31(19)	C(33)-C(32)-C(31)	119.70(19)
C(3)-C(4)-C(5)	118.06(18)	C(17)-C(18)-H(18)	119.8	C(33)-C(32)-H(32)	120.1
N(1)-C(4)-C(5)	120.26(17)	C(19)-C(18)-H(18)	119.8	C(31)-C(32)-H(32)	120.1
C(6)-C(5)-C(4)	120.87(19)	C(18)-C(19)-C(20)	119.9(2)	C(34)-C(33)-C(32)	120.41(19)
C(6)-C(5)-H(5)	119.6	C(18)-C(19)-H(19)	120	C(34)-C(33)-H(33)	119.8
C(4)-C(5)-H(5)	119.6	C(20)-C(19)-H(19)	120	C(32)-C(33)-H(33)	119.8
C(5)-C(6)-C(7)	121.63(18)	C(21)-C(20)-C(19)	119.8(2)	C(33)-C(34)-C(35)	119.94(19)
C(5)-C(6)-H(6)	119.2	C(21)-C(20)-H(20)	120.1	C(33)-C(34)-H(34)	120
C(7)-C(6)-H(6)	119.2	C(19)-C(20)-H(20)	120.1	C(35)-C(34)-H(34)	120
C(2)-C(7)-C(6)	116.62(18)	C(20)-C(21)-C(16)	120.02(18)	C(34)-C(35)-C(36)	120.21(19)
C(2)-C(7)-C(8)	117.98(19)	C(20)-C(21)-N(1)	120.96(17)	C(34)-C(35)-H(35)	119.9
C(6)-C(7)-C(8)	125.34(18)	C(16)-C(21)-N(1)	119.01(17)	C(36)-C(35)-H(35)	119.9
C(9)-C(8)-C(7)	121.12(19)	O(3)-C(22)-O(4)	116.3(2)	C(35)-C(36)-C(31)	119.76(18)
C(9)-C(8)-H(8)	119.4	O(3)-C(22)-C(30)	126.9(2)	C(35)-C(36)-S(2)	121.07(15)
C(7)-C(8)-H(8)	119.4	O(4)-C(22)-C(30)	116.80(18)	C(31)-C(36)-S(2)	119.14(15)

C(8)-C(9)-C(1)	121.4(2)	C(23)-O(4)-C(22)	122.12(16)	C(37)-S(2)-C(36)	97.52(9)
C(8)-C(9)-H(9)	119.3	C(24)-C(23)-O(4)	116.59(16)	C(42)-C(37)-C(38)	119.71(18)
C(1)-C(9)-H(9)	119.3	C(24)-C(23)-C(28)	122.96(17)	C(42)-C(37)-S(2)	119.25(14)
C(4)-N(1)-C(10)	119.22(15)	O(4)-C(23)-C(28)	120.44(17)	C(38)-C(37)-S(2)	121.03(15)
C(4)-N(1)-C(21)	118.79(15)	C(23)-C(24)-C(25)	119.53(17)	C(39)-C(38)-C(37)	119.72(19)
C(10)-N(1)-C(21)	113.40(15)	C(23)-C(24)-H(24)	120.2	C(39)-C(38)-H(38)	120.1
C(11)-C(10)-C(15)	119.96(19)	C(25)-C(24)-H(24)	120.2	C(37)-C(38)-H(38)	120.1
C(11)-C(10)-N(1)	120.99(19)	C(24)-C(25)-N(2)	120.79(17)	C(38)-C(39)-C(40)	120.51(19)
C(15)-C(10)-N(1)	119.03(17)	C(24)-C(25)-C(26)	118.48(17)	C(38)-C(39)-H(39)	119.7
C(12)-C(11)-C(10)	119.8(2)	N(2)-C(25)-C(26)	120.73(17)	C(40)-C(39)-H(39)	119.7
C(12)-C(11)-H(11)	120.1	C(27)-C(26)-C(25)	120.68(18)	C(39)-C(40)-C(41)	119.97(19)
C(10)-C(11)-H(11)	120.1	C(27)-C(26)-H(26)	119.7	C(39)-C(40)-H(40)	120
C(13)-C(12)-C(11)	120.2(2)	C(25)-C(26)-H(26)	119.7	C(41)-C(40)-H(40)	120
C(13)-C(12)-H(12)	119.9	C(26)-C(27)-C(28)	121.66(18)	C(40)-C(41)-C(42)	120.09(19)
C(11)-C(12)-H(12)	119.9	C(26)-C(27)-H(27)	119.2	C(40)-C(41)-H(41)	120
C(12)-C(13)-C(14)	120.5(2)	C(28)-C(27)-H(27)	119.2	C(42)-C(41)-H(41)	120
C(12)-C(13)-H(13)	119.8	C(27)-C(28)-C(23)	116.69(17)	C(41)-C(42)-C(37)	119.96(17)
C(14)-C(13)-H(13)	119.8	C(27)-C(28)-C(29)	125.33(18)	C(41)-C(42)-N(2)	121.06(17)
C(13)-C(14)-C(15)	119.9(2)	C(23)-C(28)-C(29)	117.98(18)	C(37)-C(42)-N(2)	118.94(17)
C(13)-C(14)-H(14)	120.1	C(30)-C(29)-C(28)	121.06(19)		
C(15)-C(14)-H(14)	120.1	C(30)-C(29)-H(29)	119.5		

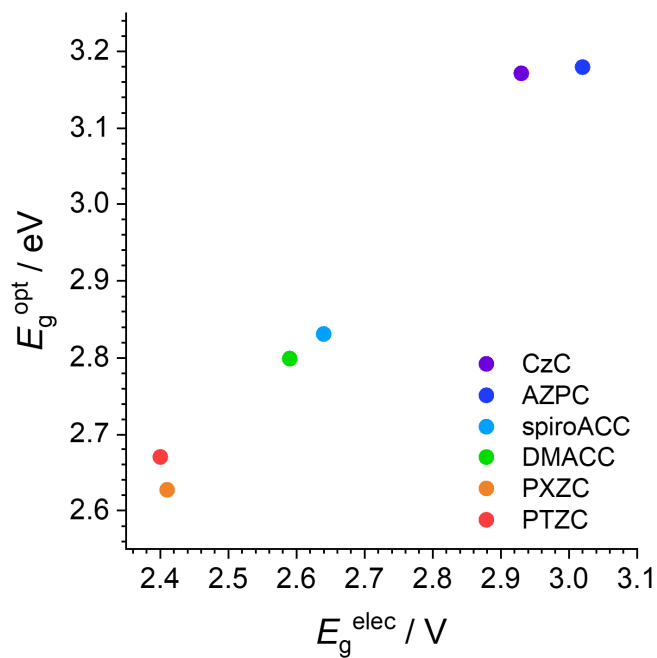


**Fig. S1** Correlation between optical ( $E_g^{\text{opt}}$ ) and electrochemical ( $E_g^{\text{elec}}$ ) band gap energies (i.e.,  $e \cdot [E_{\text{red}} - E_{\text{ox}}]$ ) of the dyads.

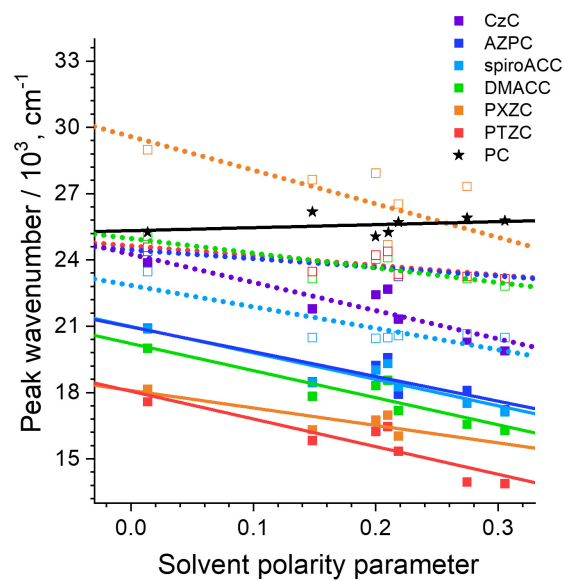


**Fig. S2** The Lippert-Mataga plots of the fluorescence emission of PC, CzC, AZPC, spiroACC, DMACC, PXZC, and PTZC: Empty squares, short-wavelength emission; filled squares, long-wavelength emission. Solvent polarity parameter ( $f$ ): solvent polarity parameter ( $f$ ): toluene, 0.0135; chloroform, 0.148; ethyl acetate, 0.200; 2-methyltetrahydrofuran, 0.210;  $\text{CH}_2\text{Cl}_2$ , 0.218; DMF, 0.275;  $\text{CH}_3\text{CN}$ , 0.305.

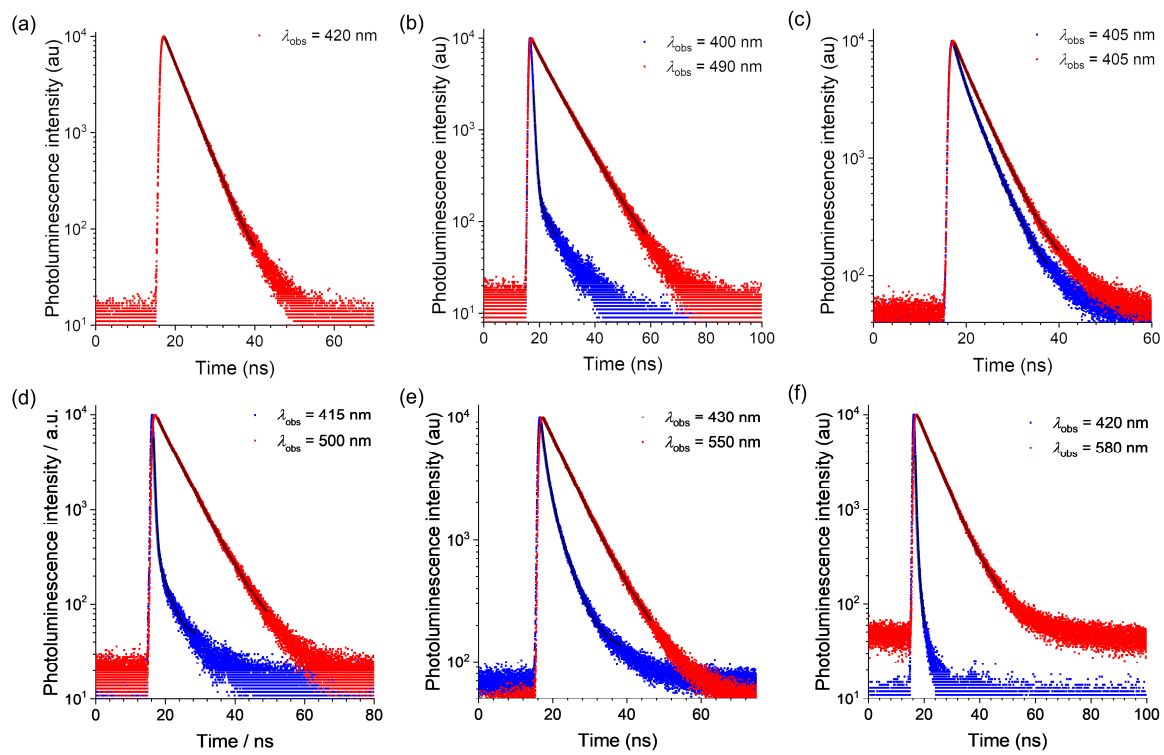


**Fig. S3** Photoluminescence decay traces of the SW (blue) and LW (red) emissions of dyads (50  $\mu\text{M}$  in Ar-saturated toluene) obtained after pulsed laser excitation at 345 nm. (a) CzC, (b) AZPC, (c) spiroACC, (d) DMACC, (e) PXZC, and (f) PTZC. The black curves show non-linear least-squares fits of the decay traces to a multi-exponential decay model. Fit results are summarized in Table 1 in the main text.

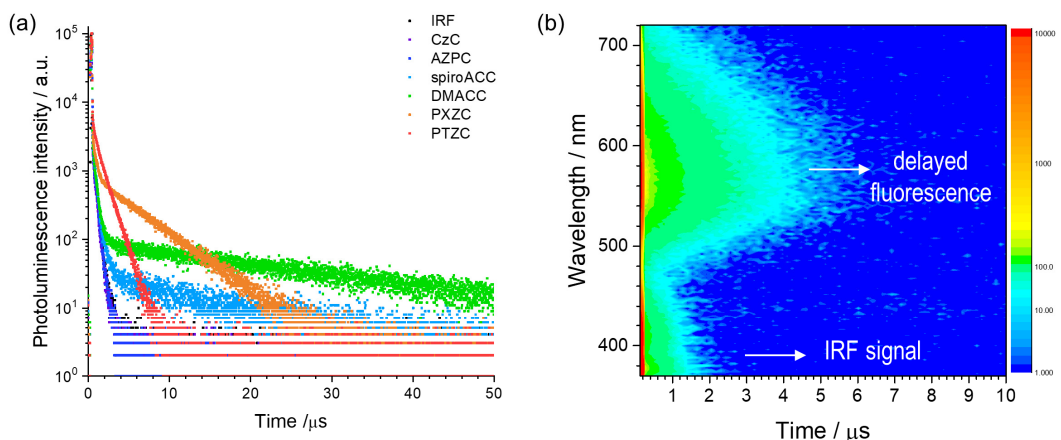


**Fig. S4** (a) Photoluminescence decay traces of the long-wavelength emissions of dyads (50  $\mu$ M in Ar-saturated toluene) obtained after picosecond pulsed laser excitation at 377 nm. (b) Time-resolved emission spectrum of PTZC (50  $\mu$ M in Ar-saturated toluene) obtained after picosecond pulsed laser excitation at 377 nm.

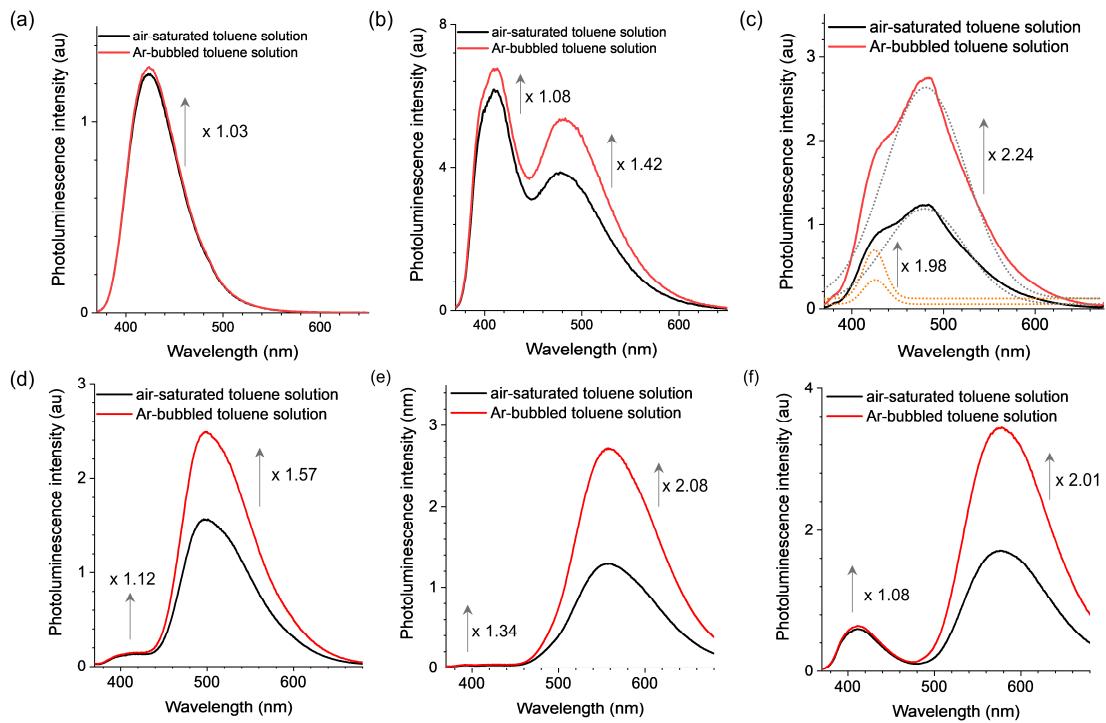


**Fig. S5** Photoluminescence spectra of the dyads ( $10 \mu\text{M}$  in toluene) obtained before (black) and after (red) deaeration: (a) CzC, (b) AZPC, (c) spiroACC, (d) DMACC, (e) PXZC, and (f) PTZC. The gray and orange dotted lines in (c) are the deconvoluted spectra of the LW and SW emissions, respectively.

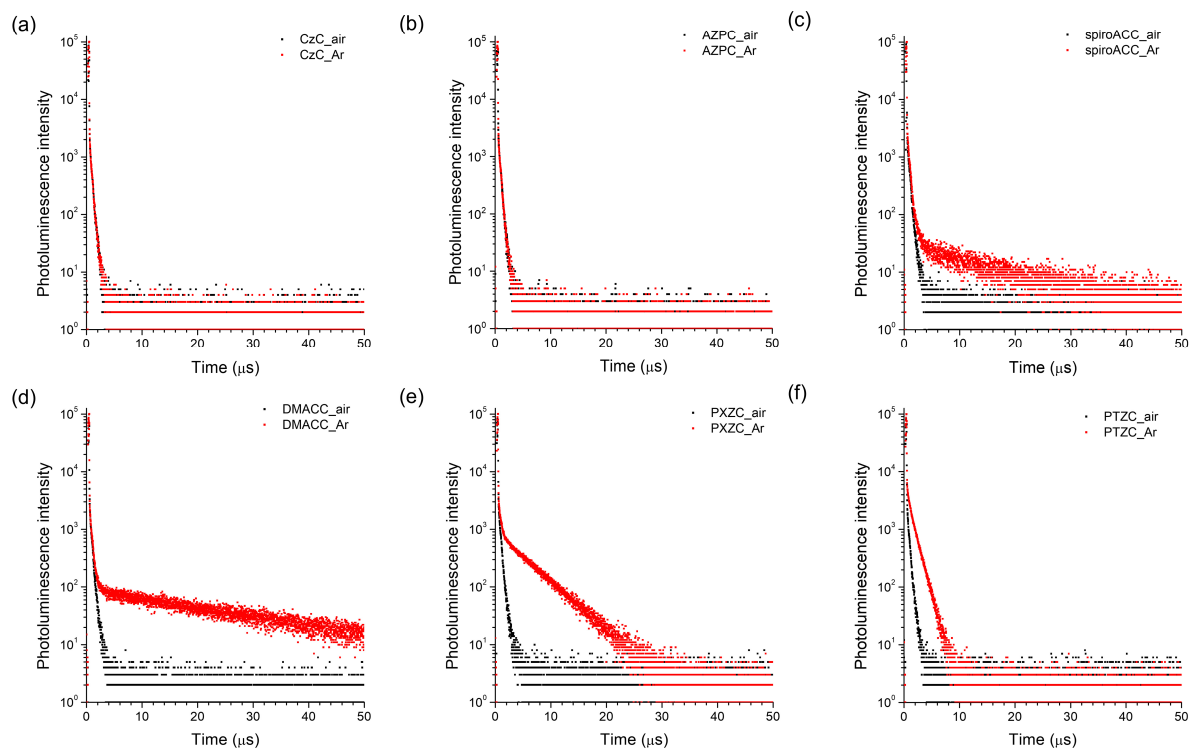


**Fig. S6** Photoluminescence decay traces of the LW emission of dyads ( $50 \mu\text{M}$  in Ar-saturated toluene) obtained before (black) and after (red) deaeration under pulsed laser excitation at 377 nm. (a) CzC, (b) AZPC, (c) spiroACC, (d) DMACC, (e) PXZC, and (f) PTZC.

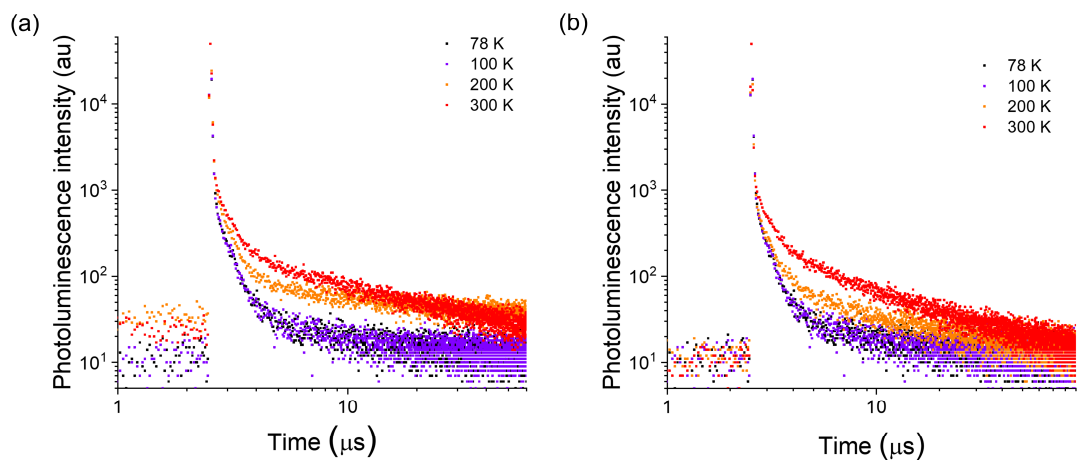


**Fig. S7** Variable-temperature fluorescence decay traces of the LW emission of (a) PXZC and (b) PTZC (5 wt % in poly(methyl methacrylate) films) acquired after 377 nm pulsed laser excitation (temporal resolution, 16 ns).

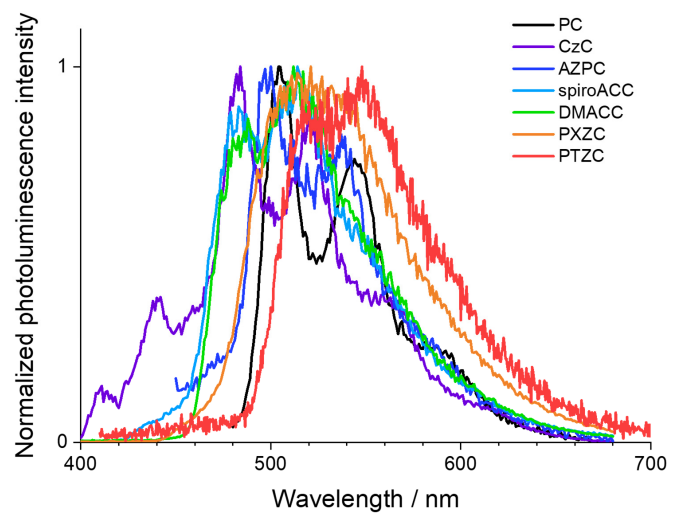


**Fig. S8** Phosphorescence spectra of dyads ( $50 \mu\text{M}$  in iodoethane or 2-MeTHF) recorded after 10 ms delay at 77 K.

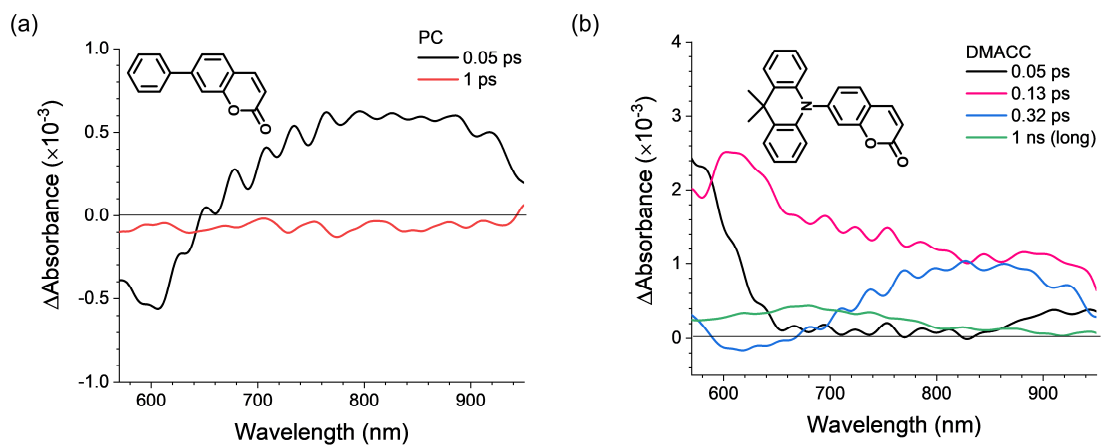


**Fig. S9** Femtosecond transient absorption spectra of toluene solutions containing (a) PC and (b) DMACC recorded after femtosecond pulsed laser excitation at 350 nm.

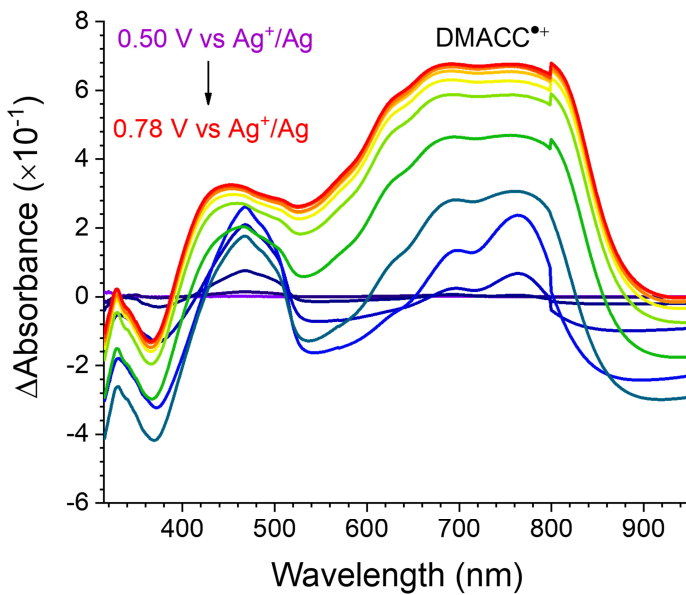


**Fig. S10** UV–Vis–NIR absorption difference spectra of 2.0 mM DMACC (Ar-saturated acetonitrile containing 0.10 M TBAPF<sub>6</sub> supporting electrolyte) recorded upon application of an anodic potential of 0.50–0.78 V vs Ag<sup>+</sup>/Ag (scan rate = 0.4 mV s<sup>-1</sup>). A Pt mesh and a Pt wire were used for the working and counter electrodes, respectively. An Ag/AgNO<sub>3</sub> pseudo reference electrode was used.

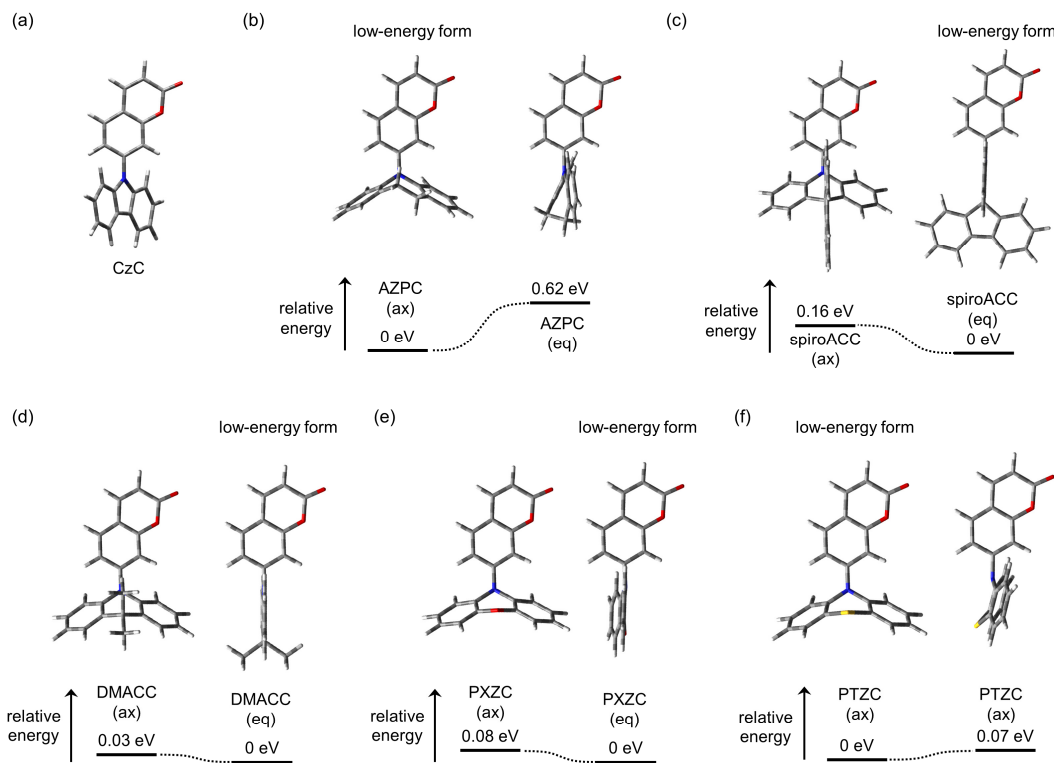


**Fig. S11** Optimized (B3LYP/6-311+G(d,p)) geometries and their energies of pseudo-axial (ax) and pseudo-equatorial (eq) conformations of (a) CzC, (b) AZPC, (c) spiroACC, (d) DMACC, (e) PXZC, and (f) PTZC. The energy value is indicated relatively to that of the lower-energy conformer.

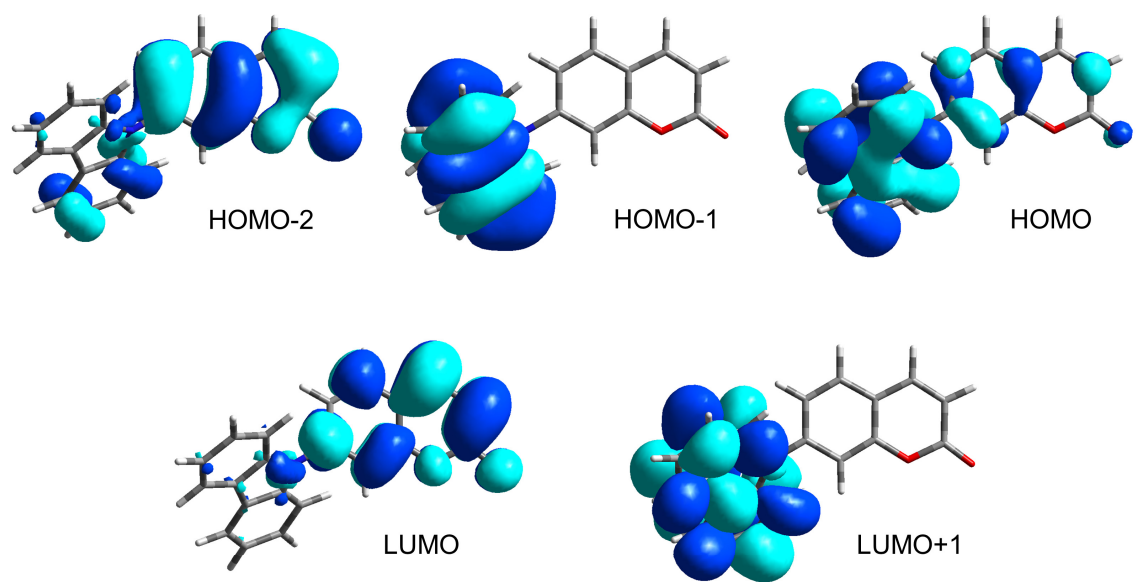


**Fig. S12.** Isosurface plots (isovalue = 0.02) of several molecular orbitals of CzC.

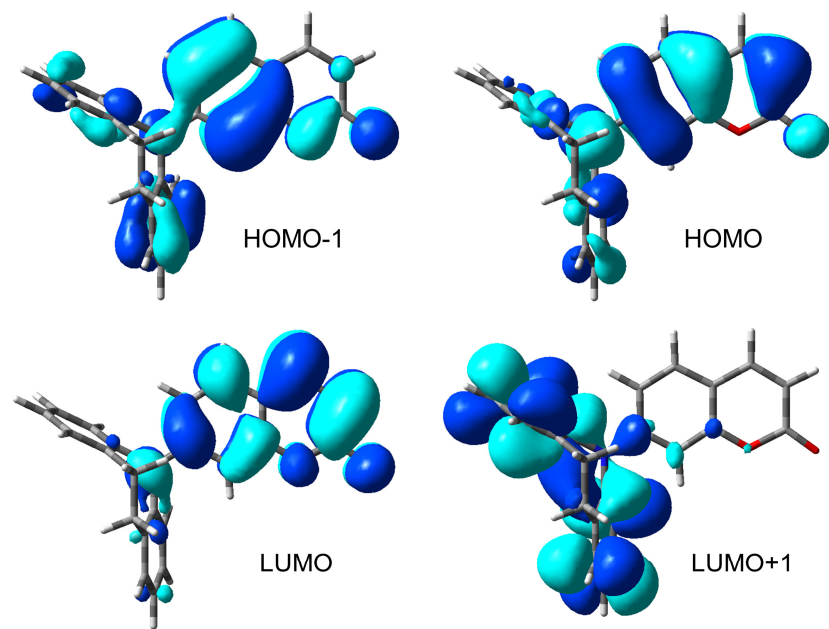


**Fig. S13** Isosurface plots (isovalue = 0.02) of several molecular orbitals of the pseudo-axial conformer of AZPC.

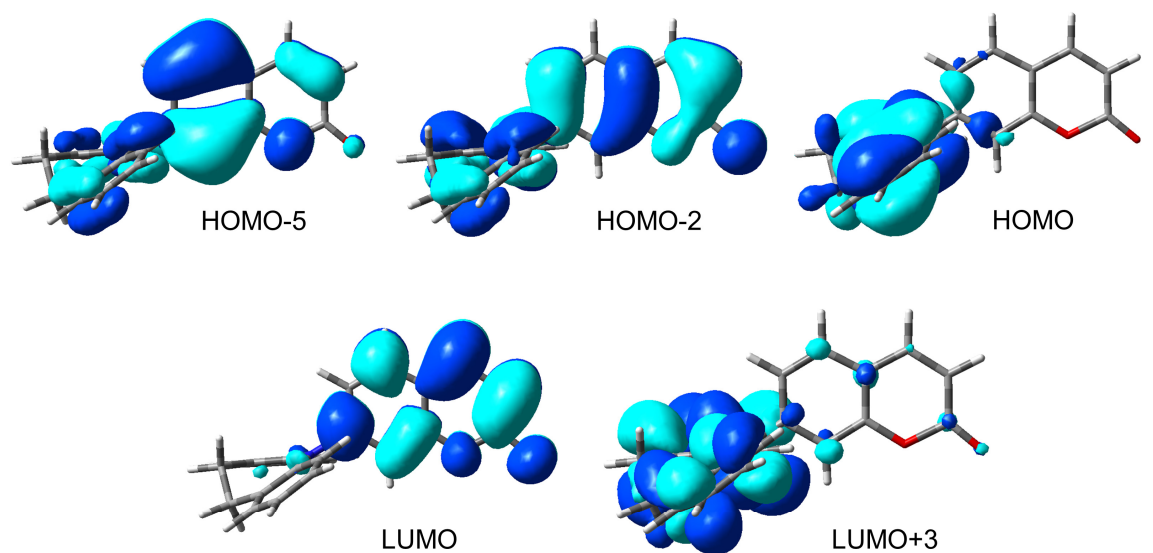


**Fig. S14** Isosurface plots (isovalue = 0.02) of several molecular orbitals of the pseudo-equatorial conformer of AZPC.

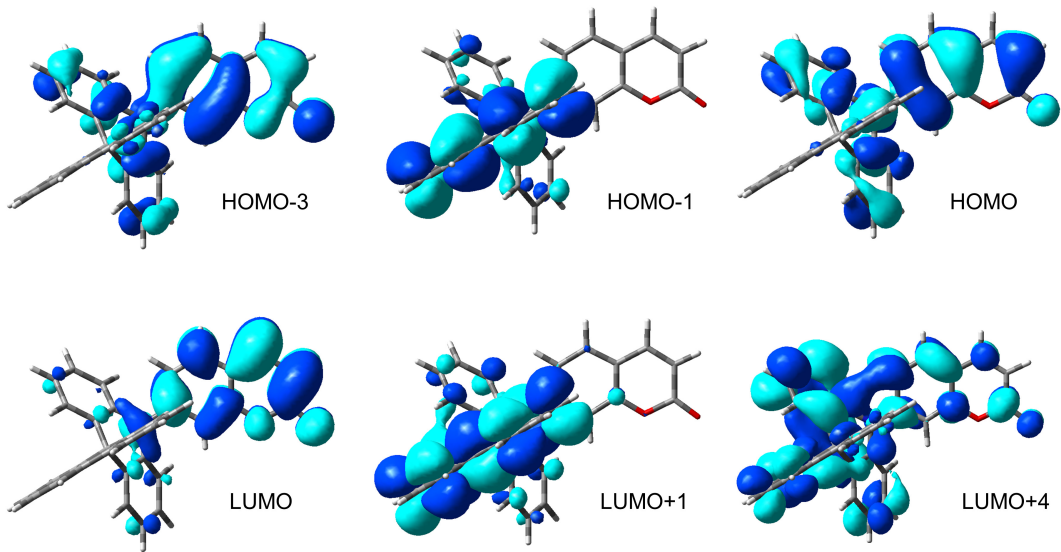


**Fig. S15** Isosurface plots (isovalue = 0.02) of several molecular orbitals of the pseudo-axial conformer of spiroACC.

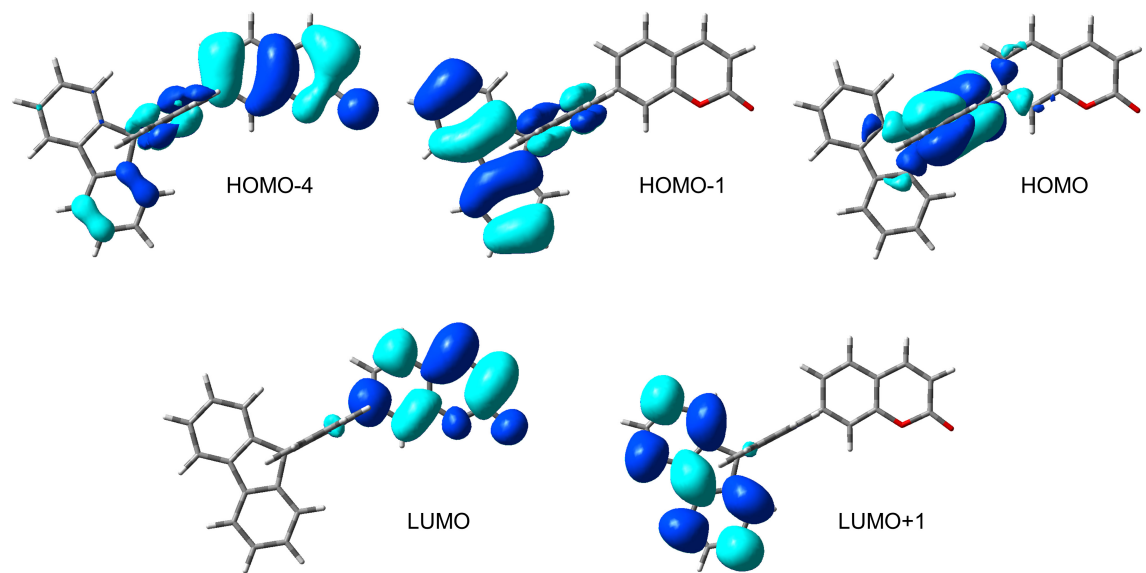


**Fig. S16** Isosurface plots (isovalue = 0.02) of several molecular orbitals of the pseudo-equatorial conformer of spiroACC.

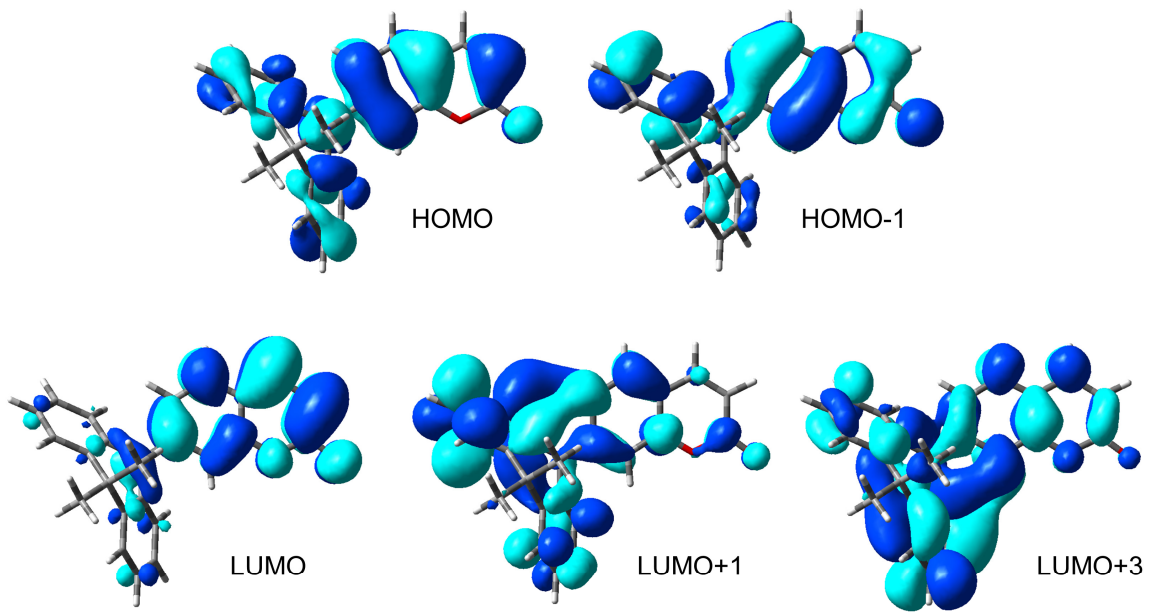


**Fig. S17** Isosurface plots (isovalue = 0.02) of several molecular orbitals of the pseudo-axial conformer of DMACC.

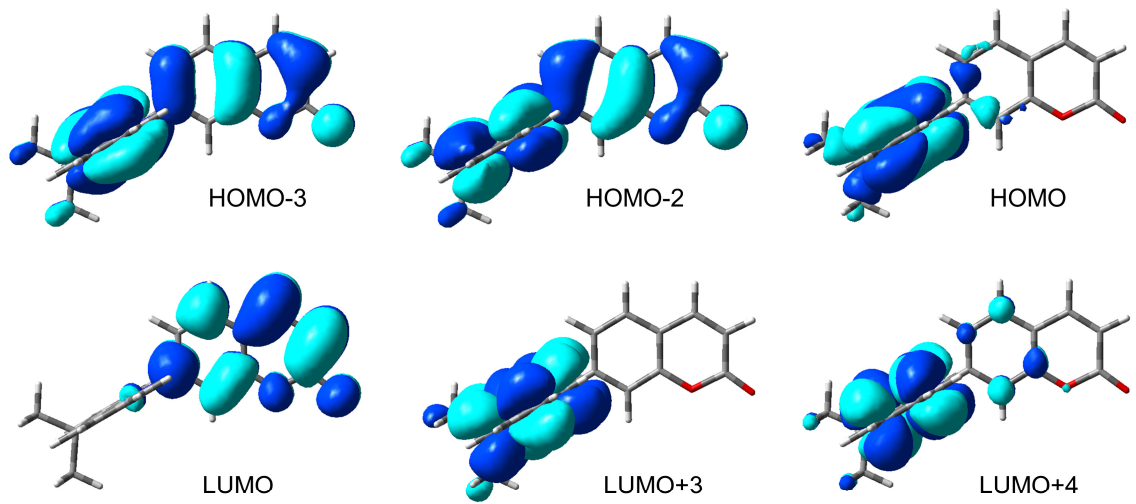


**Fig. S18** Isosurface plots (isovalue = 0.02) of several molecular orbitals of the pseudo-equatorial conformer of DMACC.

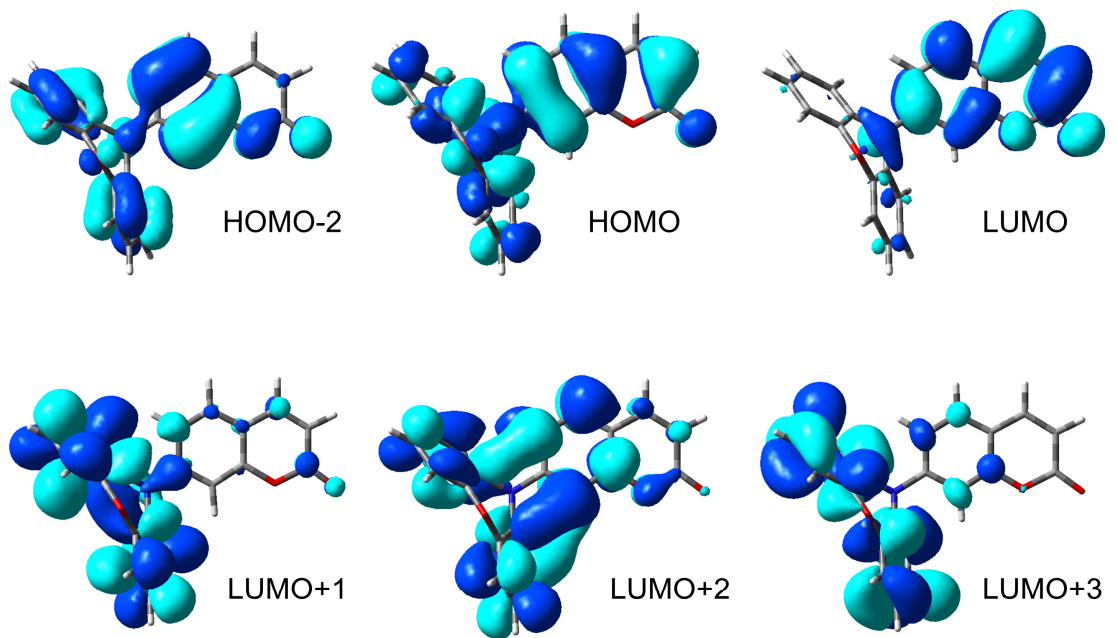


**Fig. S19** Isosurface plots (isovalue = 0.02) of several molecular orbitals of the pseudo-axial conformer of PXZC.

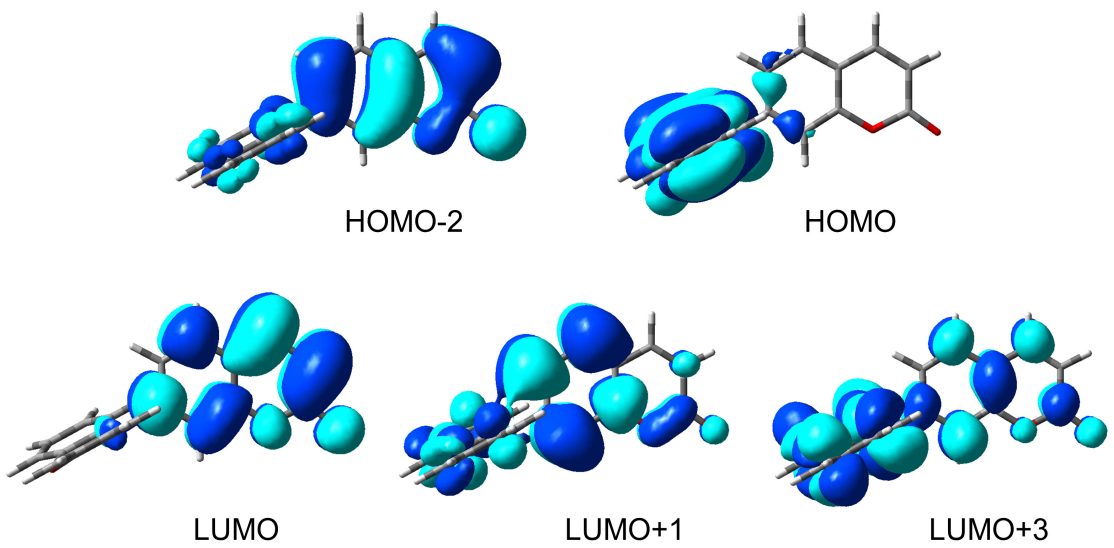


**Fig. S20** Isosurface plots (isovalue = 0.02) of several molecular orbitals of the pseudo-equatorial conformer of PXZC.

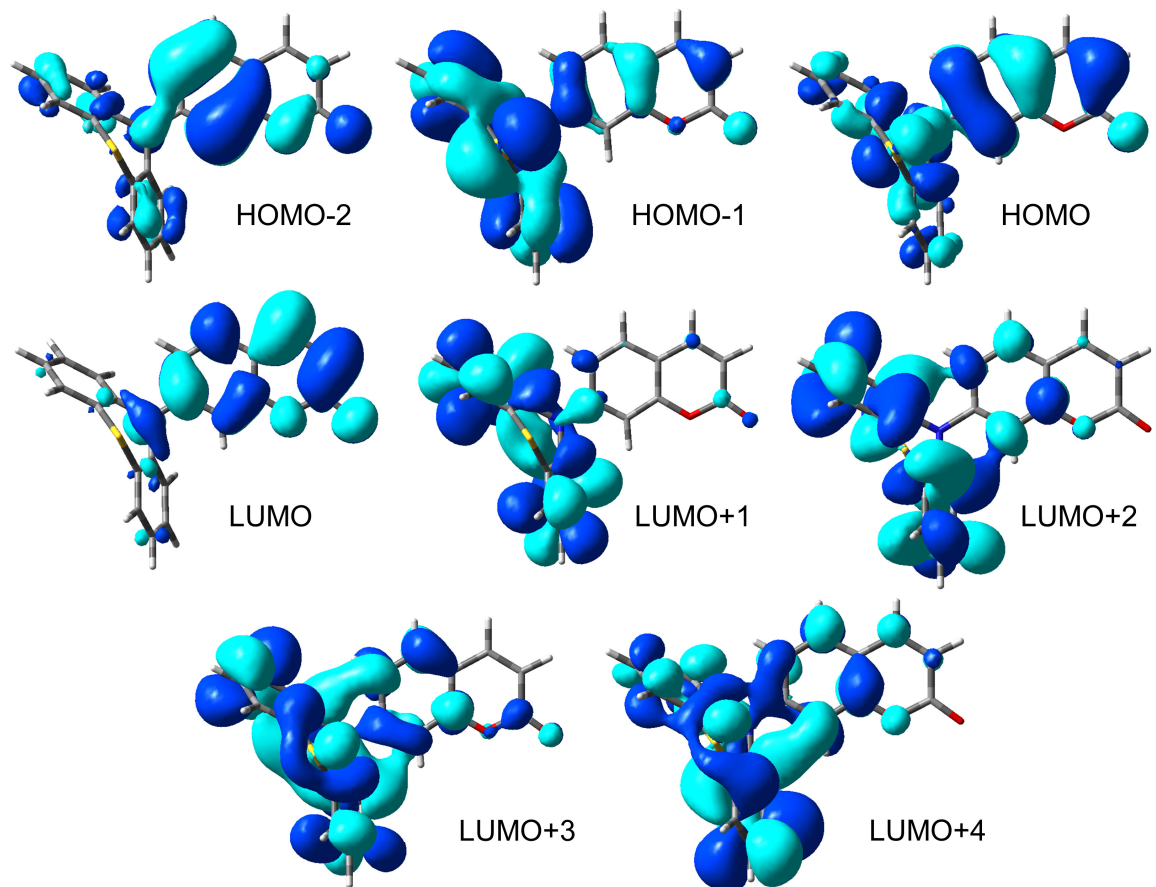


**Fig. S21** Isosurface plots (isovalue = 0.02) of several molecular orbitals of the pseudo-axial conformer of PTZC.

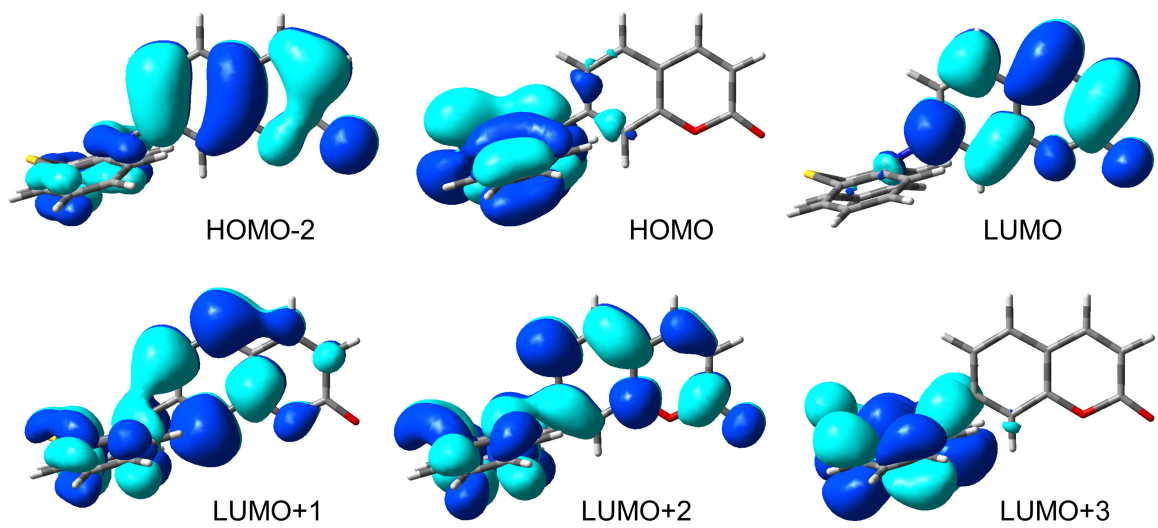


**Fig. S22** Isosurface plots (isovalue = 0.02) of several molecular orbitals of the pseudo-equatorial conformer of PTZC.

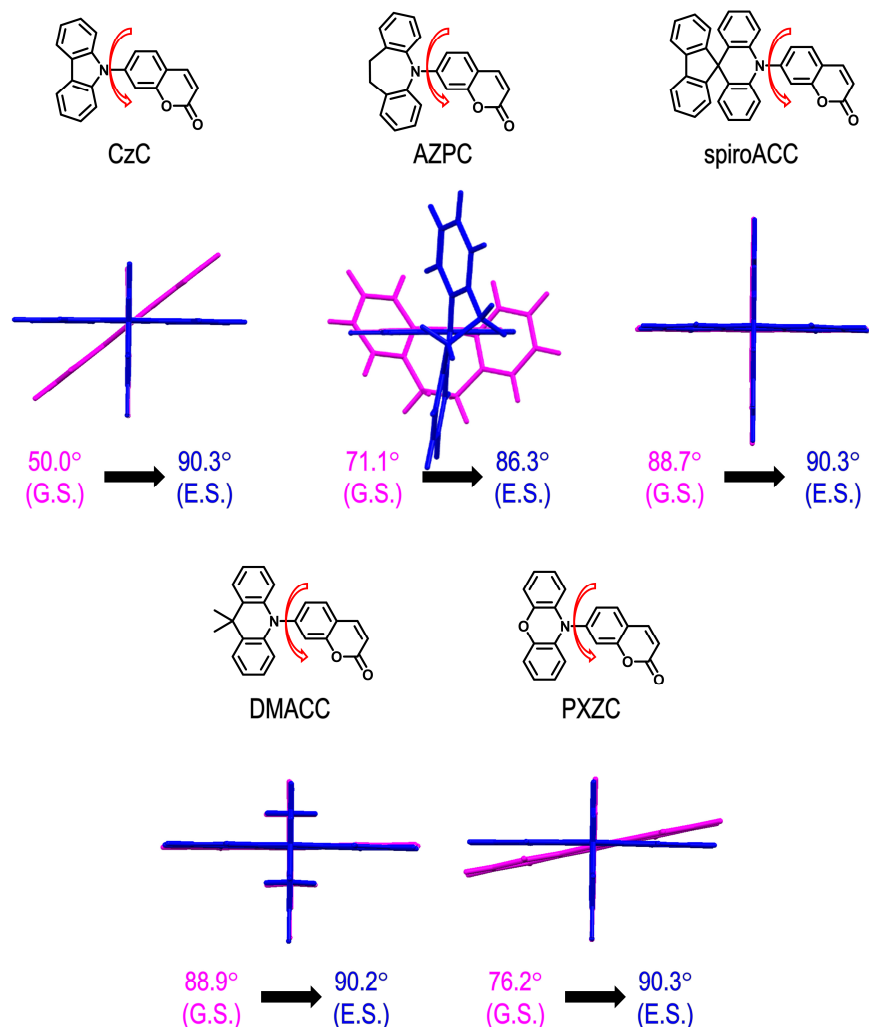


**Fig. S23** Comparison between the ground state (colored in magenta) and the first excited state geometries (colored in blue) predicted quantum chemically (B3LYP/6-311+G(d,p)). The values indicate the dihedral angle between the cyclic amino donor and coumarin.

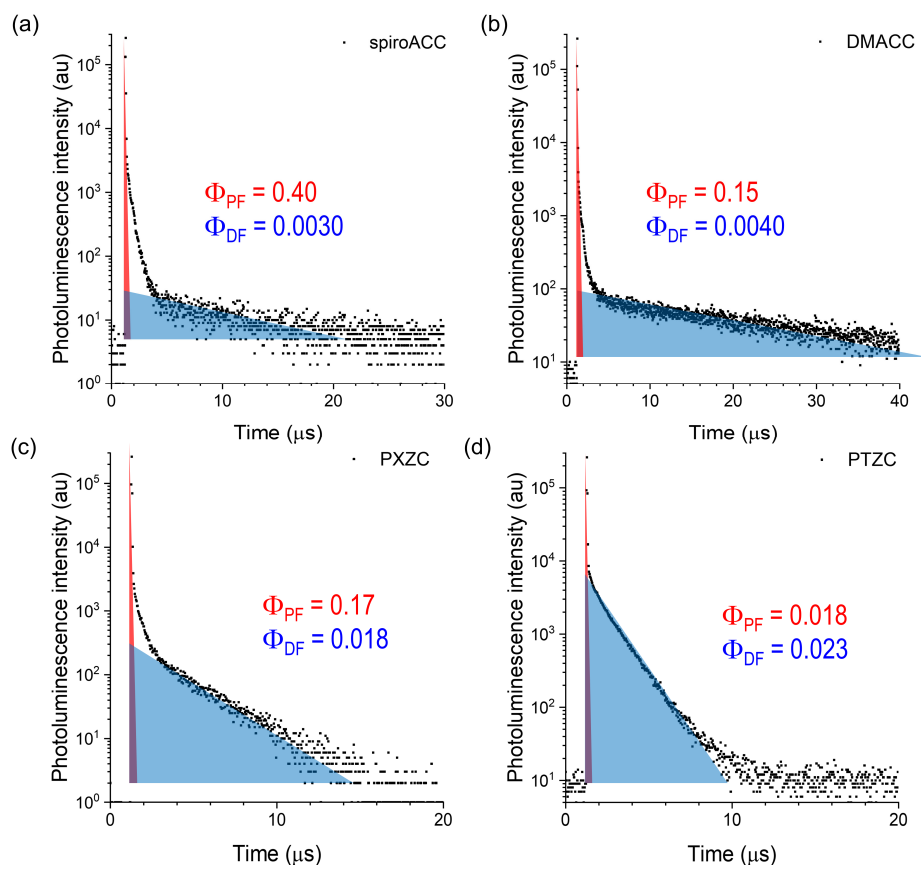


**Fig. S24** Photoluminescence decay traces of the LW emission for deoxygenated 50  $\mu$ M toluene of the DE compounds: (a) spiroACC, (b) DMACC, (c) PXZC, and (d) PTZC. The blue regions indicate the magnitude of the LW emissions.

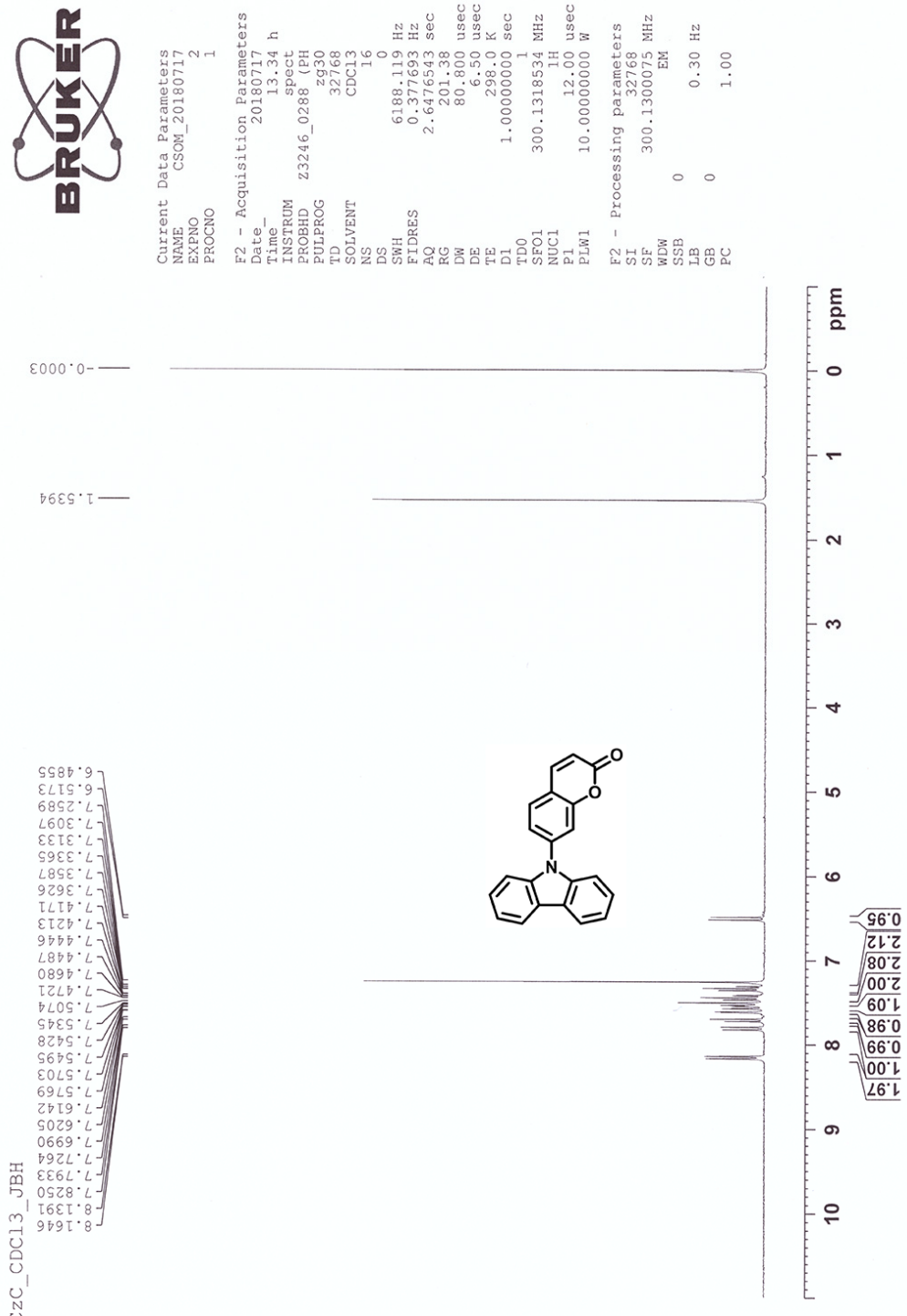


**Fig. S25** <sup>1</sup>H NMR (300 MHz, CDCl<sub>3</sub>) spectrum of CzC.

CzC / <sup>13</sup>C



서울대학교  
인조화학공동기원  
학자기공명연구실

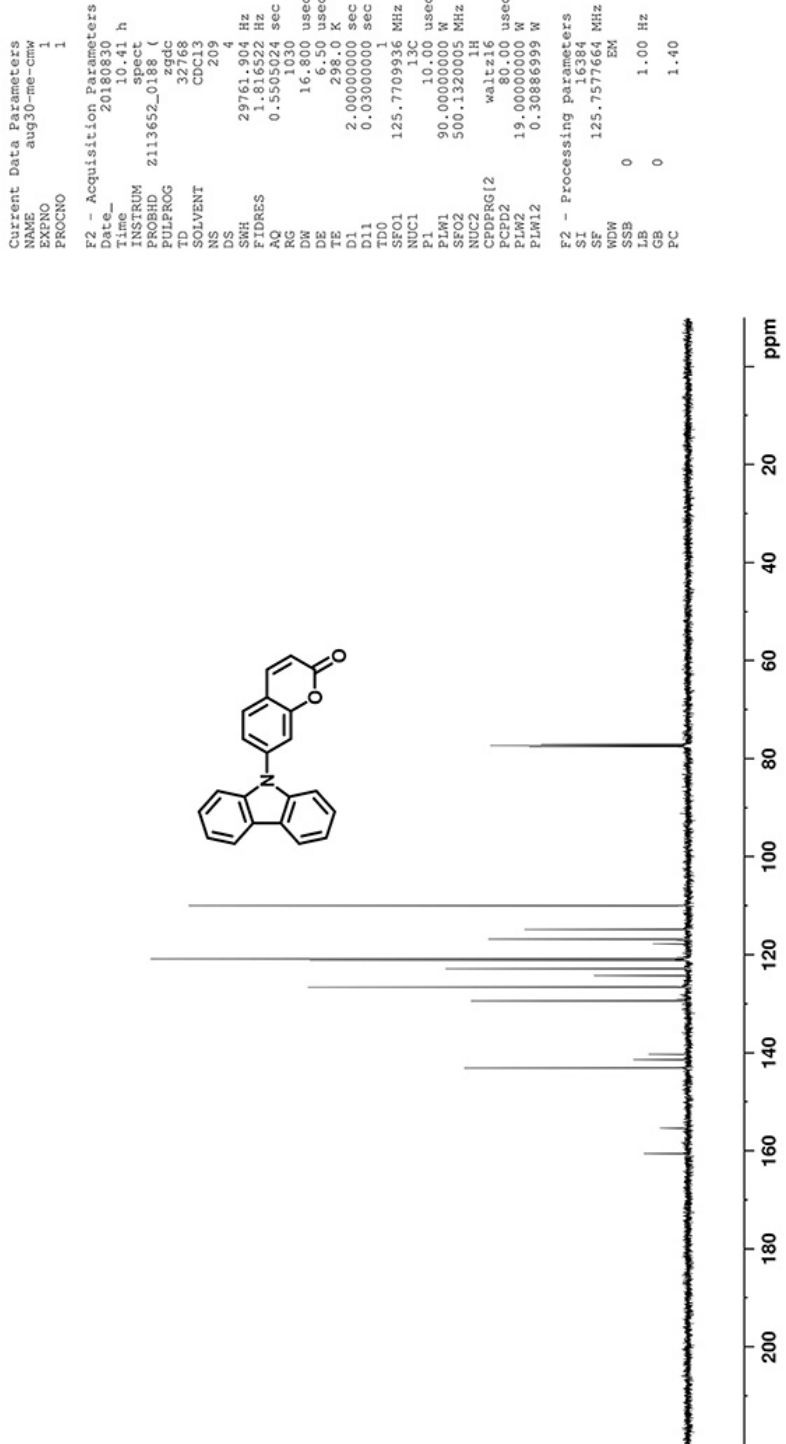
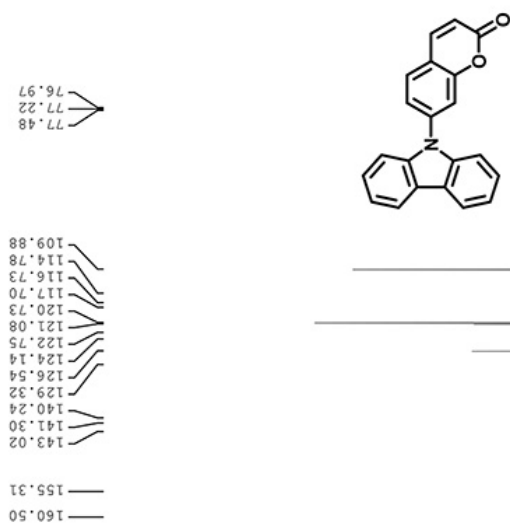
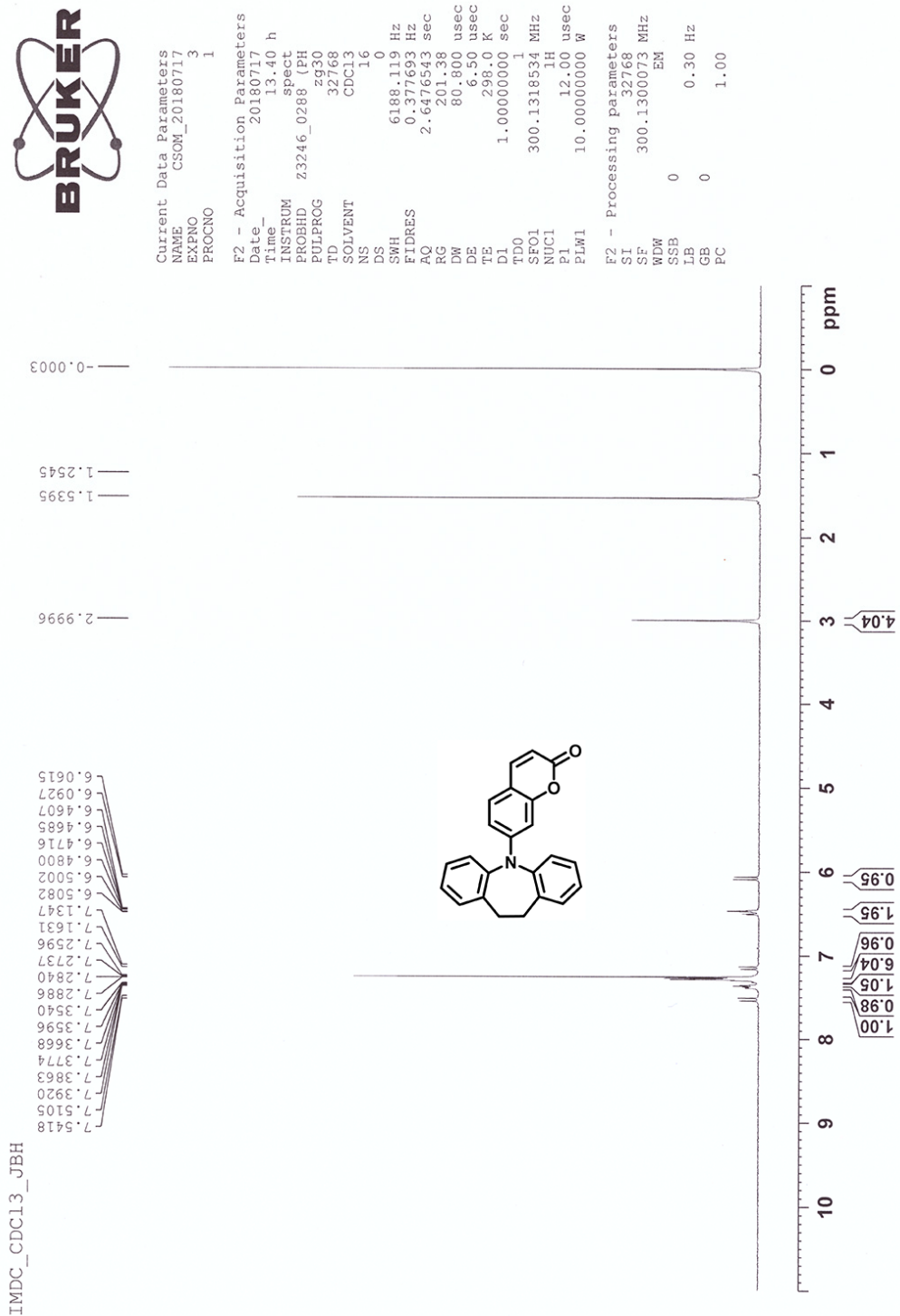
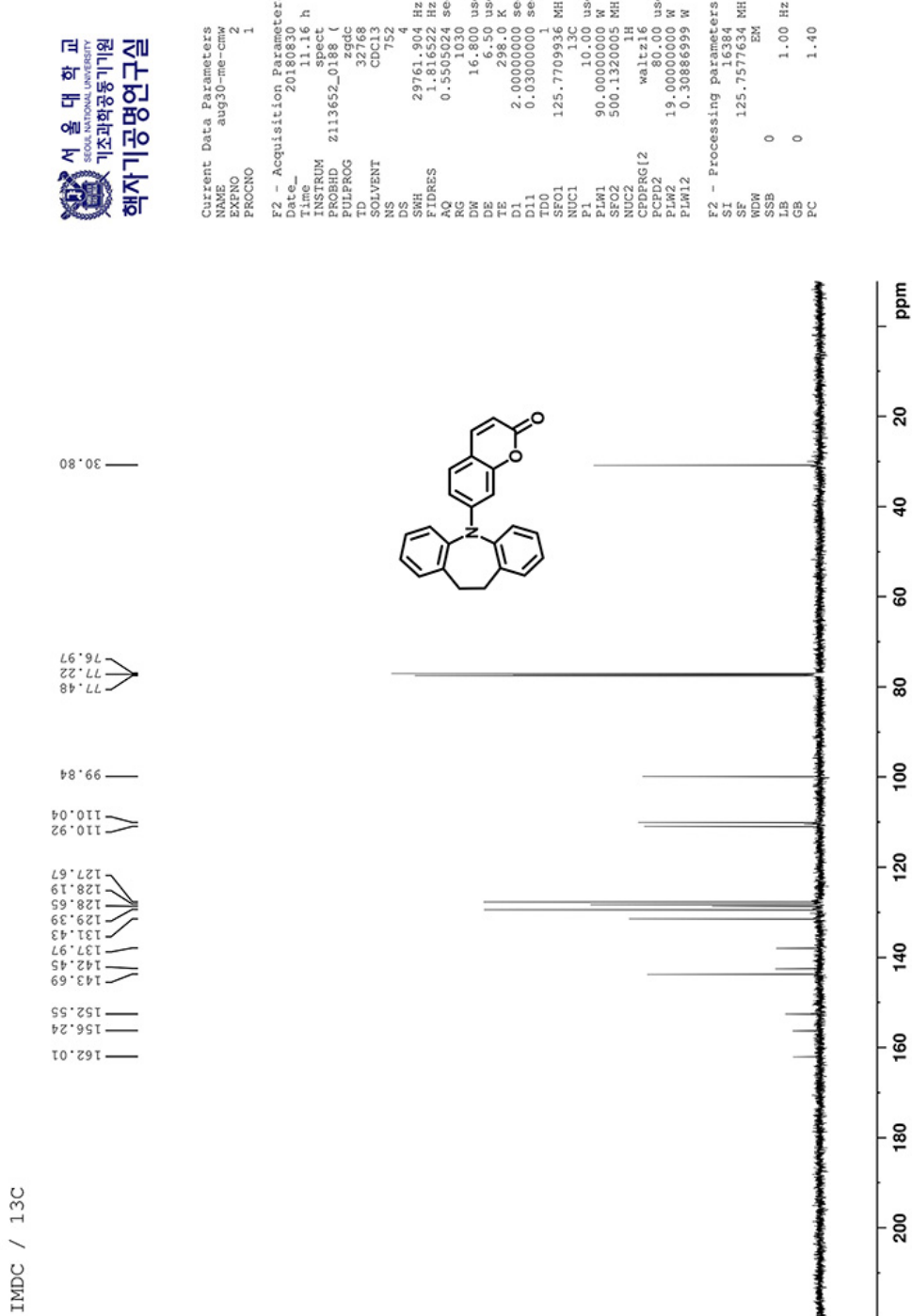


Fig. S26 <sup>13</sup>C{<sup>1</sup>H} NMR (126 MHz, CDCl<sub>3</sub>) spectrum of CzC.



**Fig. S27** <sup>1</sup>H NMR (300 MHz, CDCl<sub>3</sub>) spectrum of AZPC.

**Fig. S28**  $^{13}\text{C}\{^1\text{H}\}$  NMR (126 MHz,  $\text{CDCl}_3$ ) spectrum of AZPC.



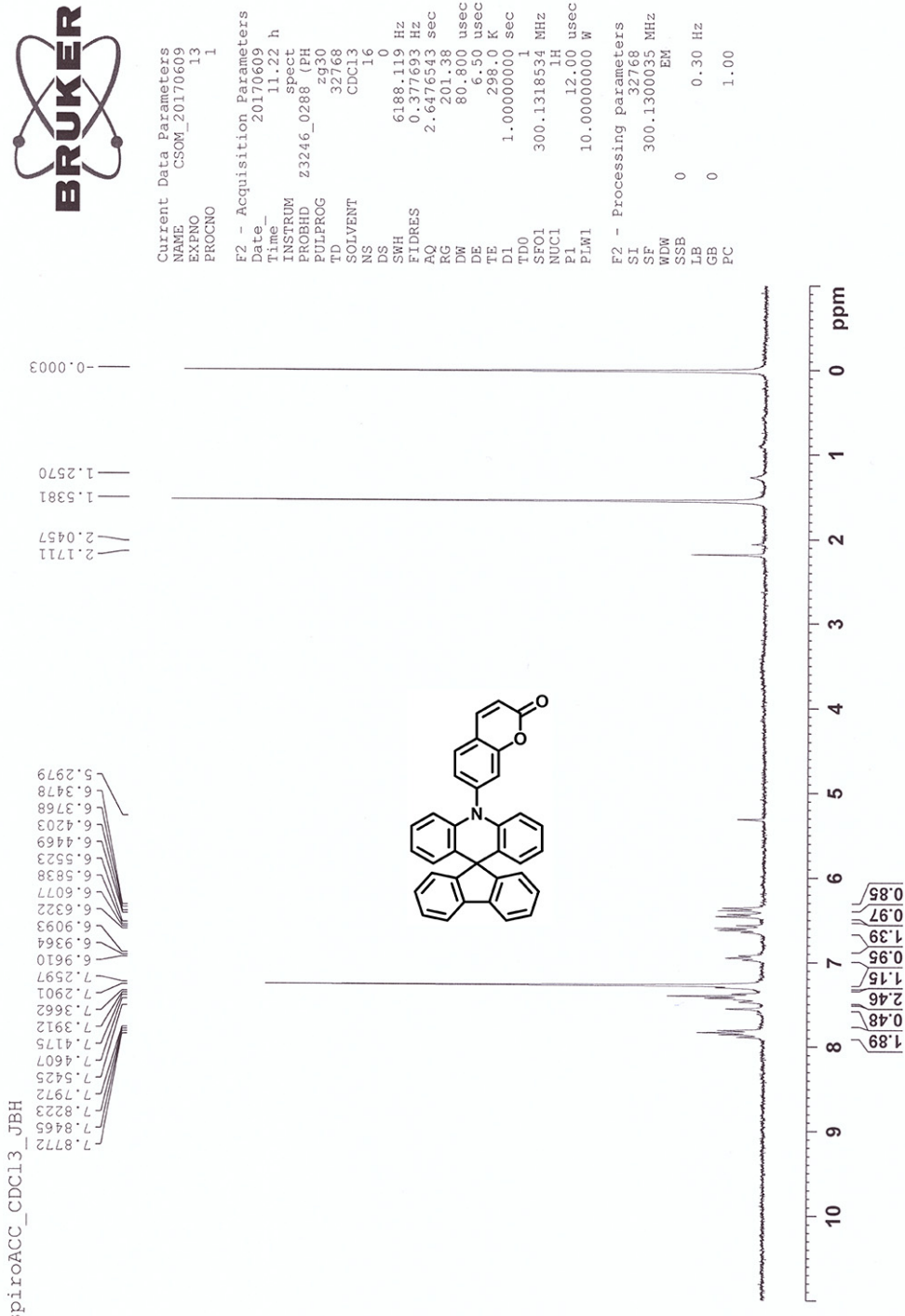


**Fig. S29** <sup>1</sup>H NMR (300 MHz, CDCl<sub>3</sub>) spectrum of spiroACC.

spiroACC /  $^{13}\text{C}$

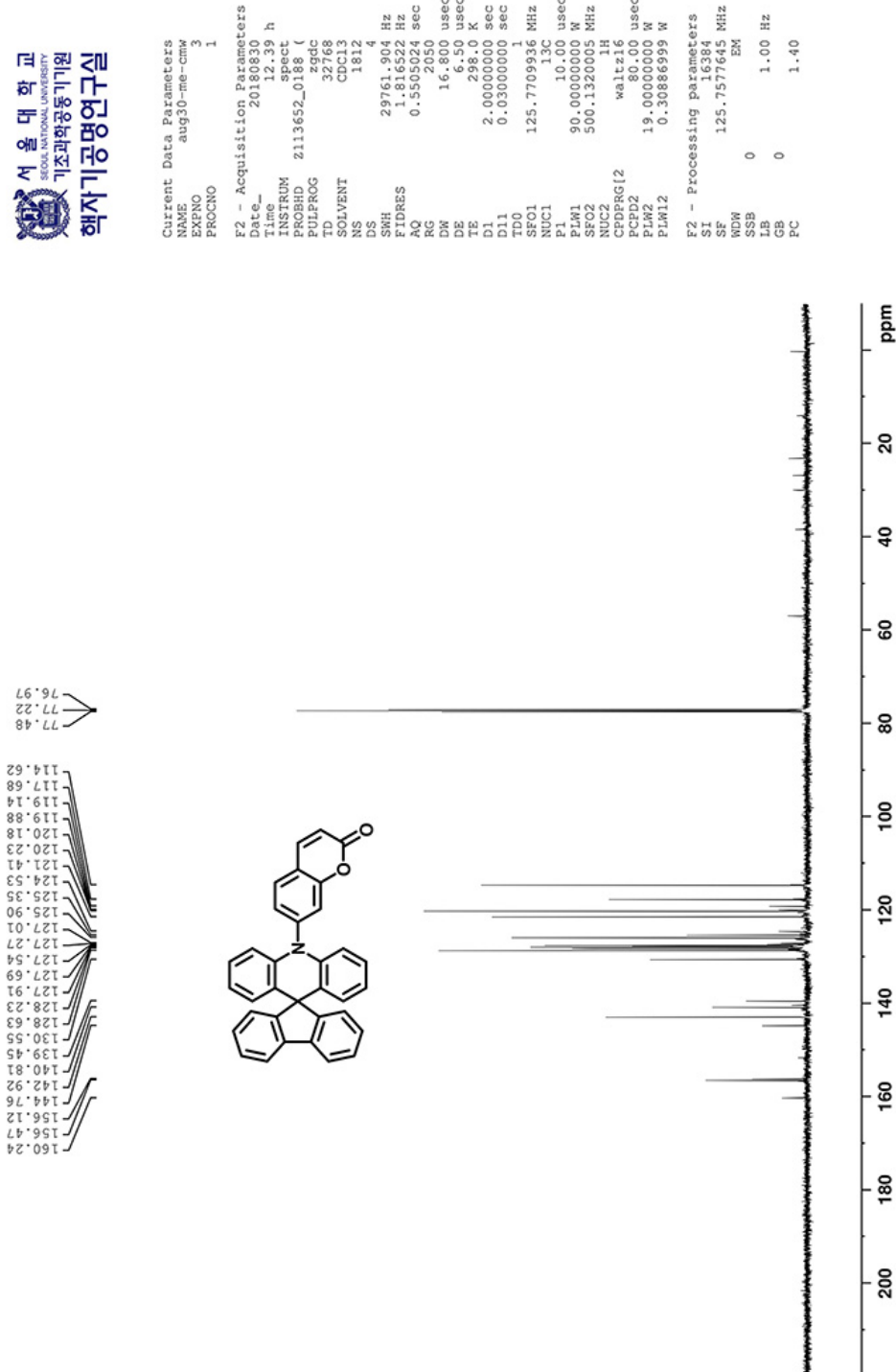


**Fig. S30**  $^{13}\text{C}\{^1\text{H}\}$  NMR (126 MHz, CDCl<sub>3</sub>) spectrum of spiroACC.

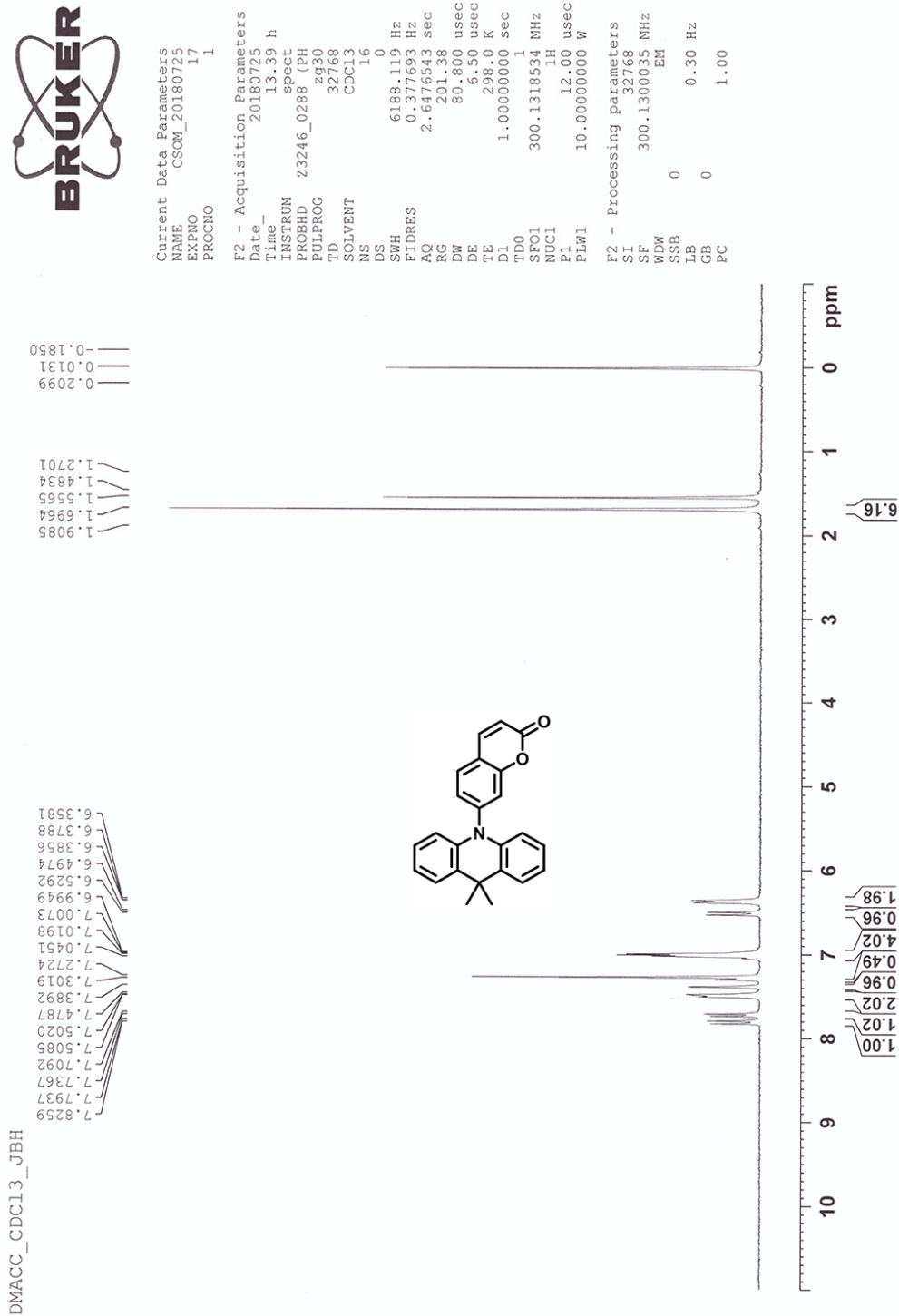
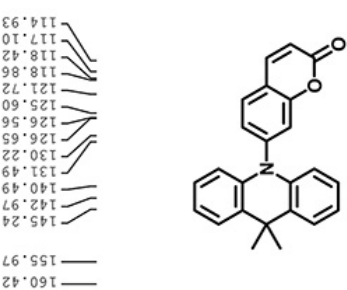


**Fig. S31** <sup>1</sup>H NMR (300 MHz, CDCl<sub>3</sub>) spectrum of DMACC.



-36.36  
-31.13

77.48  
77.23  
76.97

160.42  
155.97  
145.24  
142.97  
140.49  
131.49  
130.22  
126.65  
126.56  
121.72  
118.42  
118.86  
117.10  
114.93

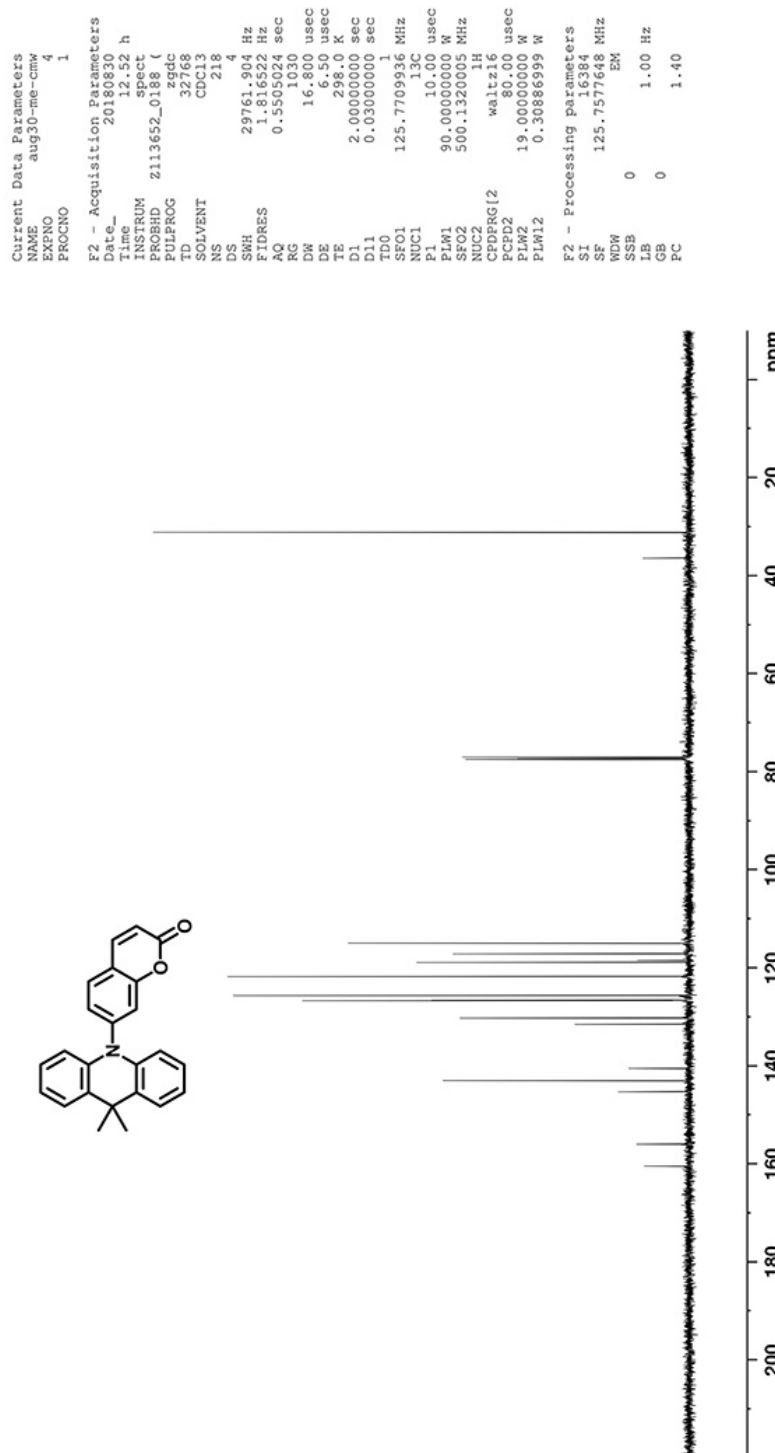


**Fig. S32**  $^{13}\text{C}\{{}^1\text{H}\}$  NMR (126 MHz,  $\text{CDCl}_3$ ) spectrum of DMACC.

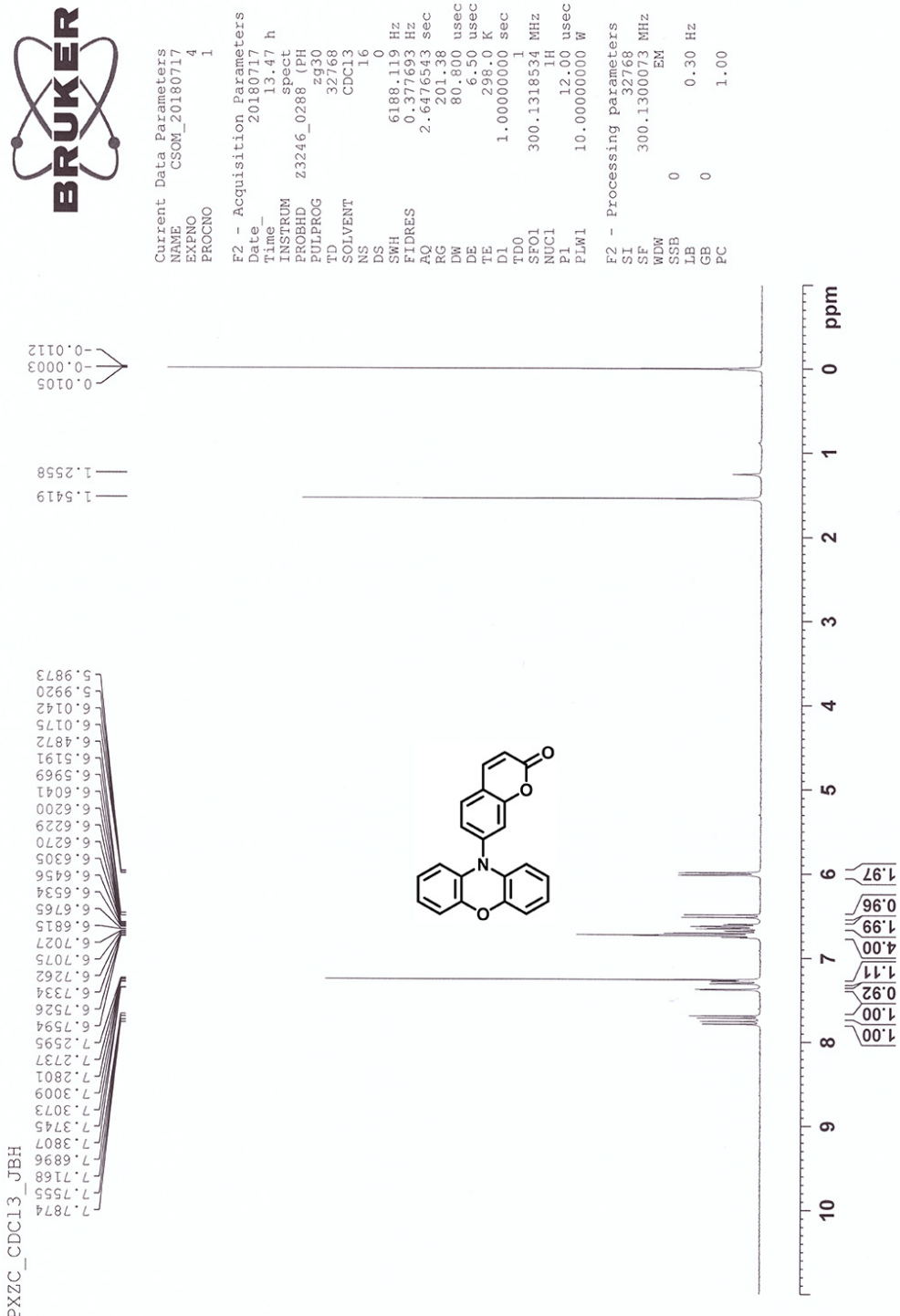


**Fig. S33** <sup>1</sup>H NMR (300 MHz, CDCl<sub>3</sub>) spectrum of PXZC.

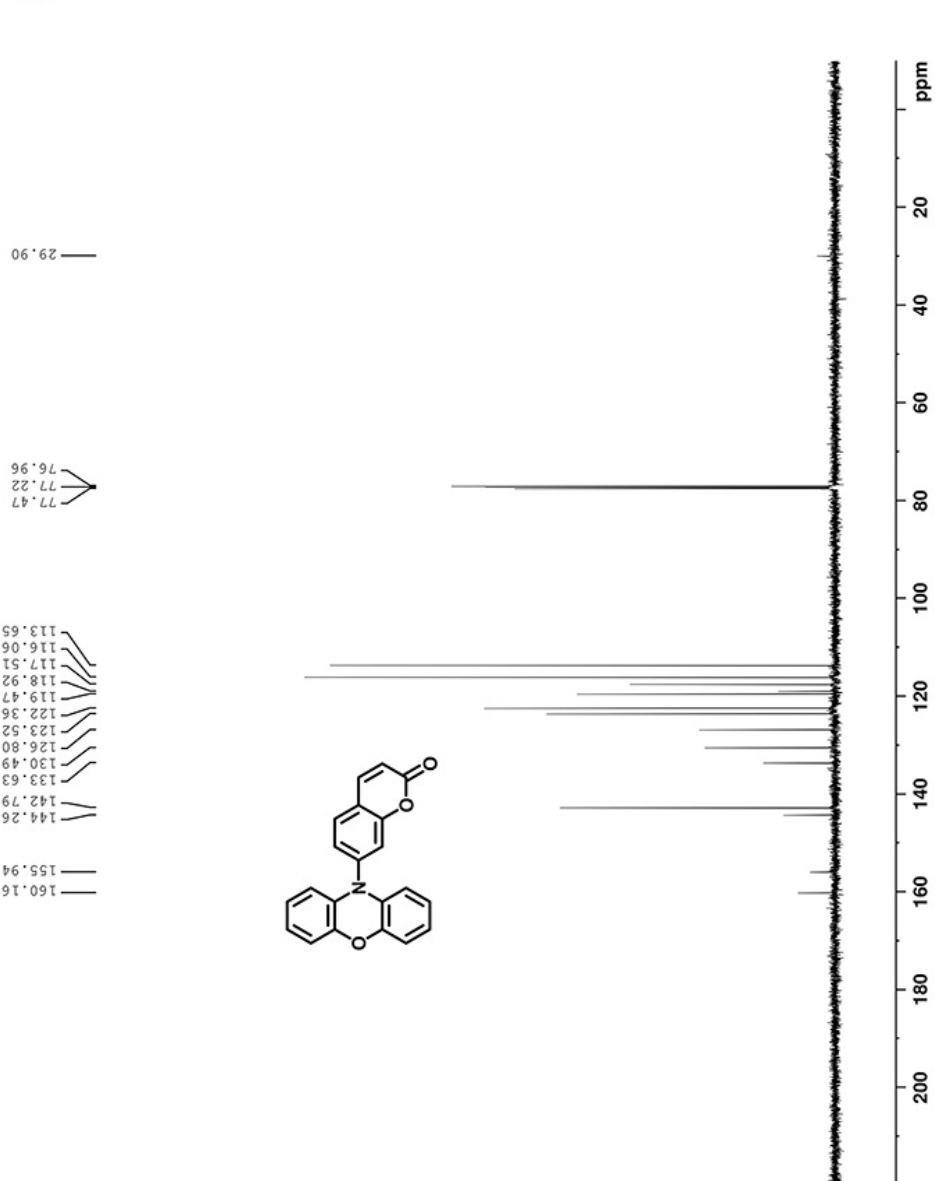


**Fig. S34**  $^{13}\text{C}\{^1\text{H}\}$  NMR (126 MHz, CDCl<sub>3</sub>) spectrum of PXZC.

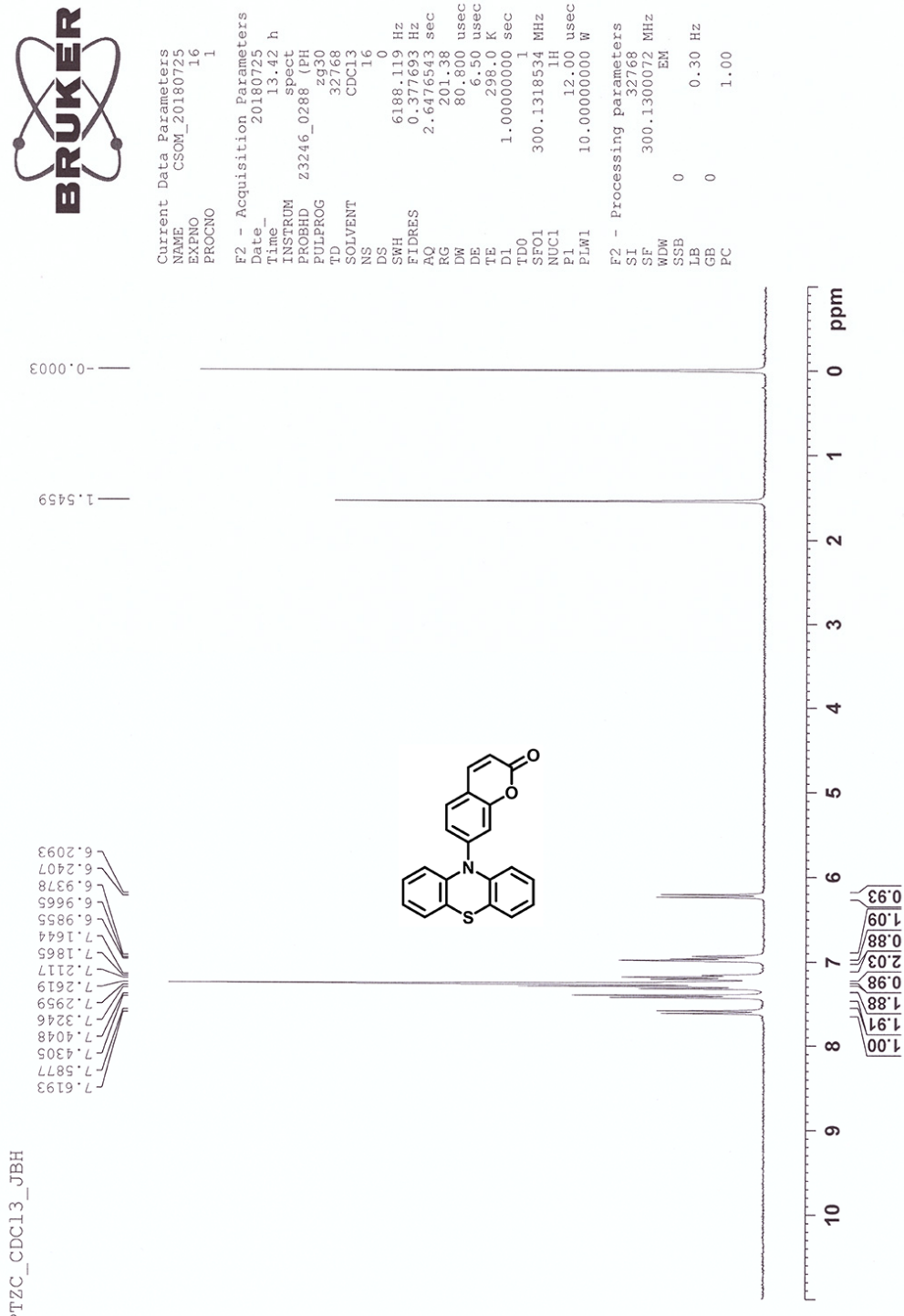


**Fig. S35** <sup>1</sup>H NMR (300 MHz, CDCl<sub>3</sub>) spectrum of PTZC.

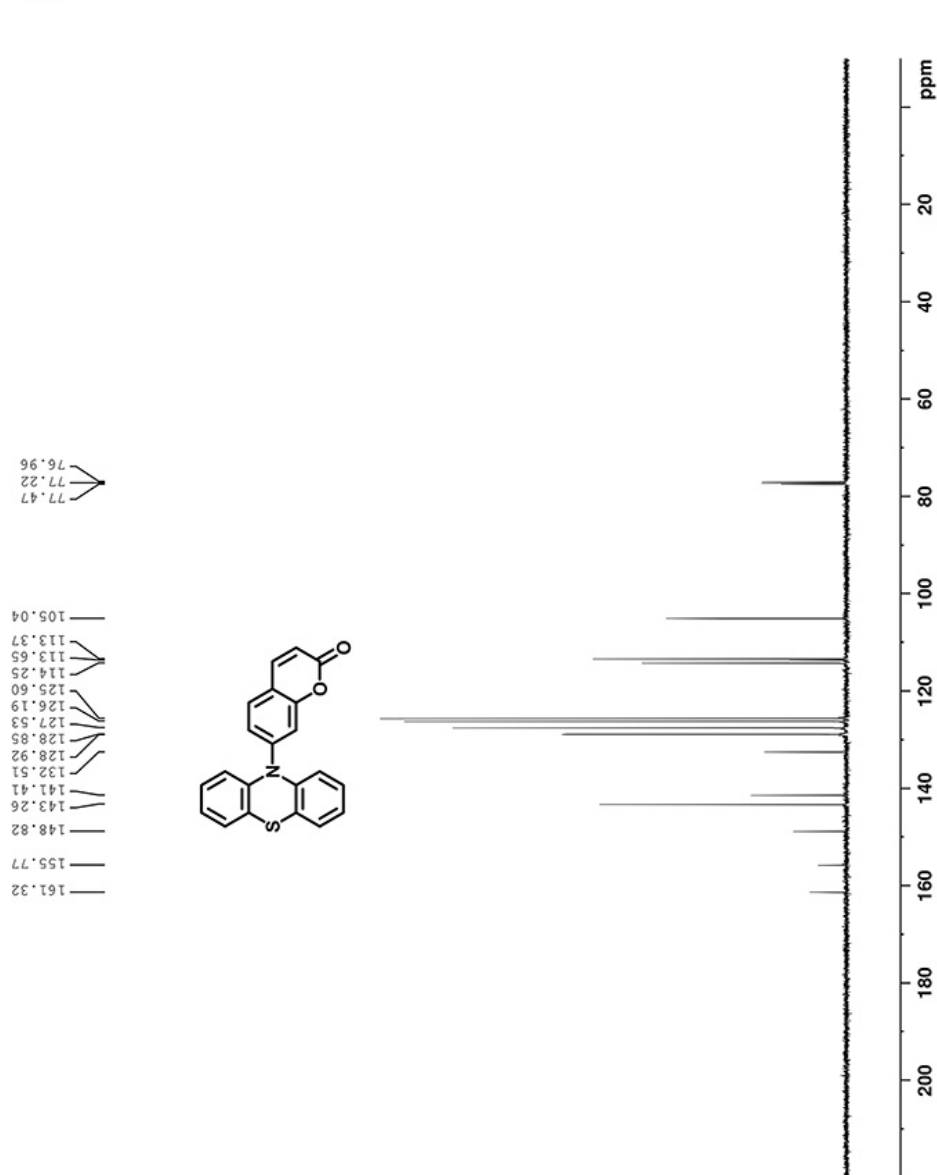


**Fig. S36**  $^{13}\text{C}\{^1\text{H}\}$  NMR (126 MHz,  $\text{CDCl}_3$ ) spectrum of PTZC.

## References

1. B. H. Jhun, K. Oukubo, S. Fukuzumi, Y. You, *J. Mater. Chem. C*, 2016, **4**, 4556-4567.
2. R. Lindner, B. van den Bosch, M. Lutz, J. N. H. Reek, J. I. van der Vlugt, *Organometallics*, 2011, **30**, 499-510.
3. M. Numata, T. Yasuda, C. Adachi, *Chem. Commun.*, 2015, **51**, 9443-9446.
4. G. Heinrich, S. Schoof, H. Gusten, *J. Photochem.*, 1974, **3**, 315-320.
5. Y. Tao, K. Yuan, T. Chen, P. Xu, H. Li, R. Chen, C. Zheng, L. Zhang, W. Huang, *Adv. Mater.* **2014**, *26*, 7931-7958.
6. I. E. Serdiuk, C. H. Ryoo, K. Kozakiewicz, M. Moříka, B. Liberek, S. Y. Park, *J. Mater. Chem. C* **2020**, *8*, 6052-6062.
7. M. J. Frisch, G. W. Trucks, H. B. Schlegel, G. E. Scuseria, M. A. Robb, J. R. Cheeseman, G. Scalmani, V. Barone, B. Mennucci, G. A. Petersson, H. Nakatsuji, M. Caricato, X. Li, H. P. Hratchian, A. F. Izmaylov, J. Bloino, G. Zheng, J. L. Sonnenberg, M. Hada, M. Ehara, K. Toyota, R. Fukuda, J. Hasegawa, M. Ishida, T. Nakajima, Y. Honda, O. Kitao, H. Nakai, T. Vreven, J. A. Montgomery, Jr., J. E. Peralta, F. Ogliaro, M. Bearpark, J. J. Heyd, E. Brothers, K. N. Kudin, V. N. Staroverov, T. Keith, R. Kobayashi, J. Normand, K. Raghavachari, A. Rendell, J. C. Burant, S. S. Iyengar, J. Tomasi, M. Cossi, N. Rega, J. M. Millam, M. Klene, J. E. Knox, J. B. Cross, V. Bakken, C. Adamo, J. Jaramillo, R. Gomperts, R. E. Stratmann, O. Yazyev, A. J. Austin, R. Cammi, C. Pomelli, J. W. Ochterski, R. L. Martin, K. Morokuma, V. G. Zakrzewski, G. A. Voth, P. Salvador, J. J. Dannenberg, S. Dapprich, A. D. Daniels, O. Farkas, J. B. Foresman, J. V. Ortiz, J. Cioslowski and D. J. Fox, Gaussian 09, Revision D.01; Gaussian, Inc.: Wallingford CT, 2009.